Triangle singularity in the production of $T_{cc}^+(3875)$ and a soft pion

Eric Braaten,[1,*] Li-Ping He,[2,†] Kevin Ingles,[1,‡] and Jun Jiang[3,§]

[1]*Department of Physics, The Ohio State University, Columbus, Ohio 43210, USA*
[2]*Helmholtz-Institut für Strahlen- und Kernphysik and Bethe Center for Theoretical Physics, Universität Bonn, D-53115 Bonn, Germany*
[3]*School of Physics, Shandong University, Jinan, Shandong 250100, China*

(Received 14 February 2022; accepted 28 July 2022; published 29 August 2022)

The double-charm tetraquark meson $T_{cc}^+(3875)$ can be produced in high-energy proton-proton collisions by the creation of the charm mesons $D^{*+}D^0$ at short distances followed by their binding into T_{cc}^+. The T_{cc}^+ can also be produced by the creation of $D^{*+}D^{*+}$ at short distances followed by their rescattering into $T_{cc}^+\pi^+$. A charm-meson triangle singularity produces a narrow peak in the $T_{cc}^+\pi^+$ invariant mass distribution 6.1 MeV above the threshold with a width of about 1 MeV. Well beyond the peak, the differential cross section decreases with the invariant kinetic energy E of $T_{cc}^+\pi^+$ as $E^{-1/2}$. The fraction of T_{cc}^+ that are accompanied by π^+ with $E < m_\pi$ is estimated to be roughly 3%. The fraction of T_{cc}^+ events with $T_{cc}^+\pi^+$ in the narrow peak from the triangle singularity could be comparable.

DOI: 10.1103/PhysRevD.106.034033

I. INTRODUCTION

The discoveries since the beginning of the 21st century of dozens of exotic heavy hadrons not predicted by the quark model have resulted in a second revolution in hadron spectroscopy [1–7]. This second revolution began with the discovery of the $X(3872)$ (also known as $\chi_{c1}(3872)$ or, more concisely, X) by the Belle Collaboration in 2003 [8]. The X has a remarkably narrow width, and it has other properties consistent with a hidden-charm tetraquark meson. A new front in the revolution was recently opened up by the discovery of the first double-charm tetraquark meson $T_{cc}^+(3875)$ (or more concisely, T_{cc}^+) by the LHCb Collaboration [9]. The width of T_{cc}^+ may be even narrower than that of the J/ψ [10], whose discovery in 1974 launched the first revolution in hadron spectroscopy [11,12]. The quark model introduced in 1964 provides a simple explanation for the patterns of most of the hadrons discovered in the 20th century, both light hadrons and heavy hadrons that contain charm and bottom quarks [13,14]. The development of quantum chromodynamics (QCD) provided a fundamental explanation for these patterns. The patterns of exotic heavy hadrons discovered in the second revolution are not yet understood. They present a major challenge to our understanding of QCD.

Until the discovery of T_{cc}^+, X was unique among the exotic heavy hadrons not only in its narrow width but also in how close it is to the threshold for a pair of hadrons to which it can couple. The mass of X is extremely close to the $D^{*0}\bar{D}^0$ scattering threshold. Recent precise measurements of its energy ε_X relative the $D^{*0}\bar{D}^0$ threshold by the LHCb Collaboration give $\varepsilon_X = -0.07 \pm 0.12$ MeV [15,16]. The J^{PC} quantum numbers of X were determined by the LHCb Collaboration in 2013 to be 1^{++} [17]. They imply that X has an S-wave coupling to $D^{*0}\bar{D}^0$. The universality of near-threshold S-wave resonances for particles with short-range interactions is therefore applicable [18]. This remarkable aspect of quantum mechanics guarantees that X has universal properties determined by ε_X [19]. The dominant component of the wave function of X is a loosely bound charm-meson molecule with flavor $(D^{*0}\bar{D}^0 + D^0\bar{D}^{*0})/\sqrt{2}$. If $\varepsilon_X < 0$ so that X is a bound state, the mean separation of the charm mesons is $\langle r \rangle = 1/\sqrt{8\mu|\varepsilon_X|}$, where μ is the reduced mass of $D^{*0}\bar{D}^0$. The measured value of ε_X implies $\langle r \rangle > 4.7$ fm at the 90% confidence level. Thus the radius of X is probably an order of magnitude larger than that of most hadrons.

The T_{cc}^+ is a second exotic heavy hadron to which the universality of near-threshold S-wave resonances is applicable. The mass of T_{cc}^+ is extremely close to the $D^{*+}D^0$ scattering threshold. The energy ε_T relative to the $D^{*+}D^0$ threshold measured by the LHCb Collaboration assuming a

*braaten.1@osu.edu
†heliping@hiskp.uni-bonn.de
‡ingles.27@buckeyemail.osu.edu
§jiangjun87@sdu.edu.cn

Breit-Wigner line shape is -273 ± 63 keV [9]. The real part ε_T of the pole energy assuming a line shape that takes into account the nearby $D^{*+}D^0$ threshold is [10]

$$\varepsilon_T = -360 \pm 40 \text{ keV}. \quad (1)$$

The analysis by the LHCb Collaboration suggests that its J^P quantum numbers are 1^+. This implies that T_{cc}^+ has an S-wave coupling to $D^{*+}D^0$. Universality then implies that the dominant component of the wave function of T_{cc}^+ is a loosely bound charm-meson molecule with flavor $D^{*+}D^0$. The mean separation of the charm mesons is $\langle r \rangle = 1/\sqrt{8\mu|\varepsilon_T|}$, where μ is the reduced mass of $D^{*+}D^0$. The measured value of ε_T implies $\langle r \rangle = 3.7 \pm 0.2$ fm, which is almost an order of magnitude larger than the radius of most hadrons.

Universality identifies the dominant components of the wave functions of X and T_{cc}^+ to be a loosely bound charm-meson molecule. The universal wave function has the form $\psi(r) = (1/r)\exp(-\gamma r)$. This universal wave function is applicable only at separations r larger than the size of a charm meson. Universality says nothing about the wave function at shorter distances. The wave function of X at shorter distances has a small $D^{*+}D^- + D^{*-}D^+$ component. It could also have a charmonium component ($c\bar{c}$) or a compact tetraquark component ($c\bar{c}q\bar{q}$). The wave function of T_{cc}^+ at shorter distances has a small $D^{*0}D^+$ component. It could also have a compact tetraquark component ($cc\bar{q}\bar{q}$) or a component with $\bar{q}\bar{q}$ bound to a heavy diquark (cc).

A physicist who is skeptical about the relevance of universality to the X and T_{cc}^+ could ask for direct experimental evidence for the large size of the loosely bound charm-meson molecule. One might hope to find evidence for the nature of X and T_{cc}^+ from their decays. However the only decays sensitive to the long-distance wave function are those with contributions from the decay of a constituent D^* or $\bar{D}^*$. In the case of the X, the only such decay modes are $D^0\bar{D}^0\pi^0$ and $D^0\bar{D}^0\gamma$. In the case of the T_{cc}^+, the only such decay modes are $D^0D^0\pi^+$, $D^+D^0\pi^0$, and $D^+D^0\gamma$. There have been several theoretical calculations of the partial decay rates into these three decay modes [20–24]. If the decay rates can be calculated sufficiently precisely, measurements of the three branching fractions could provide evidence that T_{cc}^+ is a loosely bound charm-meson molecule. There have also been several theoretical calculations of the line shape in the $D^0D^0\pi^+$ channel [25–28] and the invariant mass distributions for D^0D^0 and D^+D^0 [23,28]. Precise measurements of these distributions could also provide evidence that T_{cc}^+ is a loosely bound charm-meson molecule.

One might also hope to find evidence for the nature of X and T_{cc}^+ from their production. The production of the T_{cc}^+ at the LHC has been studied under the assumption that it proceeds by the fragmentation of a cc diquark jet [29,30] or by the coalescence of D^* and D charm mesons [30]. The production of X and T_{cc}^+ in heavy ion collisions may also provide information about their nature [31–40].

One way in which the production of a hadron can reveal its nature is through *triangle singularities*. A triangle singularity is a kinematic singularity that arises if three virtual particles that form a triangle in a Feynman diagram can all be on their mass shells simultaneously [41,42]. A triangle singularity can produce a double-log divergence in a reaction rate. The effects of triangle singularities on the production of exotic heavy mesons has been studied in Refs. [43,44]. A Feynman diagram for the production of a charm-meson molecule can have a triangle in which the vertices are (a) the creation of two charm mesons at short distances, (b) a transition between two charm mesons in which a pion or photon is emitted, and (c) the coalescence of two charm mesons into the molecule. The two charm mesons at vertex (c) can both be on shell in the limit as the binding energy goes to zero. The other charm meson in the triangle can brought on shell by tuning the momentum of the pion or photon that is emitted at vertex (b). The $\log^2$ divergence in the invariant mass distribution of the molecule and the recoiling pion or photon is smoothed out into a narrow peak by the binding energy of the molecule and by the decay widths of the charm mesons in the triangle.

The effects of triangle singularities on the production of X were first studied in Refs. [45–47]. Reference [45] showed that in the exclusive decays of a B meson into $KX\pi$, there is a narrow peak in the $X\pi$ invariant mass from a triangle singularity. A later study of that reaction in Ref. [48] took into account only one of the three possible Lorentz structures in the short-distance amplitude. Reference [46] showed that in the inclusive prompt production of $X\pi$ at a high-energy hadron collider, there is a narrow peak in the $X\pi$ invariant mass from a triangle singularity. In both B decay and prompt production, the peak in the $X\pi^+$ invariant mass is predicted to be about 6.1 MeV above the $X\pi^+$ threshold with a width of about 1 MeV. The peak in the $X\pi^0$ invariant mass is predicted to be about 7.3 MeV above the $X\pi^0$ threshold. In Ref. [47], Guo emphasized that the triangle singularity makes the line shape in $X\gamma$ strongly sensitive to the mass of X. In Ref. [49], the effect of the triangle singularity was studied in e^+e^- annihilation into $X\gamma + \pi^0$ and in $p\bar{p}$ annihilation into $X\gamma$. Back in 2006, Dubynskiy and Voloshin pointed out that in e^+e^- annihilation into $X\gamma$, there should be a narrow peak at a center-of-mass energy near the $D^{*0}\bar{D}^{*0}$ threshold [50]. The narrow peak comes from a charm-meson triangle singularity [51]. The peak is predicted to be at a center-of-mass energy near 4016 MeV with a width of about 5 MeV [51,52]. Other studies involving triangle singularities and X have appeared in Refs. [53–55].

In this paper, we study the effects of a charm-meson triangle singularity on the inclusive production of $T_{cc}^+\pi$ from the rescattering of D^*D^* created at short distances in

high-energy hadron collisions, such as proton-proton collisions at the Large Hadron Collider (LHC). In Sec. II we summarize some universal aspects of loosely bound S-wave molecules. In Sec. III we describe the effective field theory XEFT for charm mesons and pions that is applicable to loosely-bound charm-meson molecules. We give Feynman rules for the double-charm sector relevant to T_{cc}^+. In Sec. IV we discuss production of loosely bound charm-meson molecules at a hadron collider. In the subsequent sections, we apply XEFT to various cross sections at a high-energy hadron collider. In Sec. V we consider the production of two charm mesons with small relative momentum in channels without a resonance near the threshold. In Sec. VI we consider the production of $D^{*+}D^0$ with small relative momentum and the production of T_{cc}^+ without an accompanying soft pion. In Sec. VII we calculate the cross sections for producing $T_{cc}^+\pi^+$ and $T_{cc}^+\pi^0$. We show that a charm-meson triangle singularity produces narrow peaks in their invariant mass distributions about 6.1 MeV and 7.3 MeV above their thresholds, respectively. We summarize our results and discuss their implications in Sec. VIII. In Appendix A we determine the charm-meson triangle amplitudes in various limits. In Appendix B we give expressions for the triangle amplitudes in a coupled-channel model that takes into account the $D^{*0}D^+$ component of T_{cc}^+.

II. LOOSELY BOUND S-WAVE MOLECULES

If two particles with short-range interactions have an S-wave resonance extremely close to their scattering threshold, the few-body physics of those particles has universal aspects that are determined by their *scattering length* $1/\gamma$ [18]. In this section we describe the universal wave function for a bound state extremely close to the scattering threshold, and we present a coupled-channel model for the wave functions at shorter distances.

A. Universal wave function

If the resonance is a bound state with a negative energy ε relative to the scattering threshold, the inverse scattering length or *binding momentum* is $\gamma = \sqrt{2\mu|\varepsilon|}$, where μ is the reduced mass of the two particles. The normalized universal wave function of the bound state is

$$\psi(r) = \frac{\sqrt{\gamma/2\pi}}{r}\exp(-\gamma r). \tag{2}$$

This wave function diverges at the origin. The corresponding normalized momentum-space wave function is

$$\psi(k) = \frac{\sqrt{8\pi\gamma}}{k^2+\gamma^2}. \tag{3}$$

The spatial wave function at the origin can be expressed as an integral of the momentum-space wave function $\psi(r=0) = \int d^3k\psi(k)/(2\pi)^3$. This integral is ultraviolet divergent: it can be regularized by imposing a sharp momentum cutoff $|\boldsymbol{k}| < (\pi/2)\Lambda$ with $\Lambda \gg \gamma$. The resulting expression for the wave function at the origin, up to corrections that go to 0 as $\Lambda \to \infty$ is

$$\psi(r=0) = (\Lambda-\gamma)\sqrt{\gamma/2\pi}. \tag{4}$$

The ultraviolet cutoff Λ can be interpreted as the momentum scale beyond which $\psi(k)$ decreases more rapidly than the prediction $1/k^2$ from the universal wave function in Eq. (3). The wave function at the origin can be used to take into account short-distance components of the bound state that are not described explicitly.

The universal aspects of the low-energy scattering of the two particles can be described by a simple function of the complex energy E relative to the scattering threshold,

$$f(E) = \frac{1}{-\gamma+\sqrt{-2\mu E}}. \tag{5}$$

The universal elastic scattering amplitude at relative momentum k is obtained by evaluating $f(E)$ at $E = k^2/(2\mu) + i\epsilon$. By the optical theorem, the inclusive production rate from the creation of the two particles at short distances is proportional to the imaginary part of $f(E)$,

$$\mathrm{Im}[f(E+i\epsilon)] = \frac{\pi\gamma}{\mu}\delta(E+\gamma^2/2\mu) + \frac{\sqrt{2\mu E}}{\gamma^2+2\mu E}\theta(E). \tag{6}$$

The delta function comes from the production of the bound state and the theta function comes from the production of the two particles above the threshold. Given an ultraviolet cutoff Λ, the corresponding energy $\Lambda^2/(2\mu)$ can be interpreted as the energy scale beyond which the inclusive production rate no longer decreases as $E^{-1/2}$ as predicted by Eq. (6).

In the case of T_{cc}^+, the resonant S-wave channel consists of the charm mesons $D^{*+}D^0$. The energy ε_T of T_{cc}^+ relative to the $D^{*+}D^0$ threshold is given in Eq. (1). Its binding momentum is $\gamma_T = 26.4 \pm 1.5$ MeV. An order-of-magnitude estimate for the ultraviolet cutoff Λ is the pion mass m_π.

B. Model wave function at shorter distances

A sharp ultraviolet cutoff on the momentum $\boldsymbol{k}$ gives unphysical results for some observables. A simple model that is equivalent to a smooth ultraviolet cutoff can be defined by the normalized momentum-space wave function

$$\psi^{(\Lambda)}(k) = \frac{\sqrt{8\pi(\Lambda+\gamma)\Lambda\gamma}}{\Lambda-\gamma}\left(\frac{1}{k^2+\gamma^2} - \frac{1}{k^2+\Lambda^2}\right). \tag{7}$$

This regularized wave function was first applied to $X(3872)$ by Suzuki [56]. Its leading behavior at large k is

$$\psi^{(\Lambda)}(k) \to \sqrt{8\pi(\Lambda+\gamma)^3\Lambda\gamma}/k^4. \tag{8}$$

The spatial wave function at the origin is

$$\psi^{(\Lambda)}(r=0) = \sqrt{(\Lambda+\gamma)\Lambda\gamma/2\pi}. \tag{9}$$

The sharp cutoff $|\boldsymbol{k}| < (\pi/2)\Lambda$ used to calculate $\psi(r=0)$ in Eq. (4) was chosen so it would have the same limit for $\Lambda \gg \gamma$ as $\psi^{(\Lambda)}(r=0)$ in Eq. (9).

The regularized wave function in Eq. (7) is at best a model with the same momentum dependence as the universal wave function $\psi(k)$ at small k and more physical qualitative behavior at large k. In this model, the coefficient of $1/k^4$ in Eq. (8) and the wave function at the origin in Eq. (9) are both determined by the same parameter Λ. In general, there is no simple relation between these two quantities. Sensitivity to Λ in this model can reveal aspects of a problem that are sensitive to momenta much larger than γ. If the momentum scale where the EFT breaks down is identified, the model can be used to estimate the order of magnitude of short-distance effects by replacing Λ by that momentum scale.

C. Model wave function for coupled channel

There could be another S-wave channel coupled to the resonant channel that has a scattering threshold higher by an energy δ. In this case, the bound state will also have a component in the coupled channel with a smaller probability. For simplicity, we consider the case of a coupled channel consisting of particles with the same masses and a symmetry relating the two channels that is broken by the energy difference δ. We assume the symmetry requires the wave functions in the two channels to be equal at short distances. Note that this condition is not identical to requiring the wave functions in the two channels to be equal at large momenta.

The binding momentum for the coupled channel is $\gamma_{\rm cc} = \sqrt{2\mu(\delta+|\varepsilon|)}$. A simple model for the coupled-channel wave function is

$$\psi_{\rm cc}(k) = \frac{\Lambda-\gamma}{\Lambda-\gamma_{\rm cc}}\frac{\sqrt{8\pi\gamma}}{k^2+\gamma_{\rm cc}^2}. \tag{10}$$

We have chosen its normalization so that the wave function at the origin defined by a sharp ultraviolet cutoff $|\boldsymbol{k}| < (\pi/2)\Lambda$ is equal to that for the resonant channel in Eq. (4), $\psi_{\rm cc}(r=0) = \psi(r=0)$. Note that this symmetry condition at short distances is not equivalent to requiring $\psi_{\rm cc}(k)$ to approach $\psi(k)$ at large k except in the limit $\Lambda \to \infty$.

An alternative model for the coupled-channel wave function that corresponds to a smooth ultraviolet cutoff is

$$\psi_{\rm cc}^{(\Lambda)}(k) = \frac{\sqrt{8\pi(\Lambda+\gamma)\Lambda\gamma}}{\Lambda-\gamma_{cc}}\left(\frac{1}{k^2+\gamma_{\rm cc}^2}-\frac{1}{k^2+\Lambda^2}\right). \tag{11}$$

We have chosen its normalization so that the wave function at the origin is equal to that for the resonance channel in Eq. (9),

$$\psi_{\rm cc}^{(\Lambda)}(r=0) = \psi^{(\Lambda)}(r=0). \tag{12}$$

This condition could be required by a symmetry between the two channels at short distances. The relative probability for the coupled-channel wave function is

$$Z_{\rm cc} \equiv \int \frac{d^3k}{(2\pi)^3}|\psi_{\rm cc}^{(\Lambda)}(k)|^2 = \frac{(\Lambda+\gamma)\gamma}{(\Lambda+\gamma_{\rm cc})\gamma_{\rm cc}}. \tag{13}$$

This is less than 1 provided $\gamma < \gamma_{\rm cc}$.

The coupled-channel wave function $\psi_{\rm cc}^{(\Lambda)}(k)$ in Eq. (11) can be used in conjunction with the regularized wave function $\psi^{(\Lambda)}(k)$ in Eq. (7) as a qualitative model for the bound state in which these two components are described explicitly and all others are taken into account through the wave function at the origin. The total probability in the two channels can be normalized to 1 by multiplying both $\psi^{(\Lambda)}(k)$ in Eq. (7) and $\psi_{cc}^{(\Lambda)}(k)$ in Eq. (11) by $1/\sqrt{1+Z_{\rm cc}}$.

In the case of T_{cc}^+, the coupled S-wave channel consists of the charm mesons $D^{*0}D^+$. We sometimes denote this coupled channel simply by $0+$. We will assume that at short distances the resonance is in the isospin-0 combination $(D^{*+}D^0 - D^{*0}D^+)/\sqrt{2}$ of the two coupled channels. This is consistent with the observation by the LHCb Collaboration of a peak near threshold in the D^0D^+ invariant mass distribution, which can come from the $D^{*0}D^+$ component of T_{cc}^+. The possibility that the resonance has isospin 1 is disfavored by the nonobservation of peaks in the D^+D^+ and $D^+D^0\pi^+$ invariant mass distributions, which could come from $D^{*+}D^+$. In many of the analyses of the decays of T_{cc}^+, the resonance was assumed to be a linear combination of isospin 0 and isospin 1 [20,22,23,25]. In Ref. [25] a fit to the $D^0D^0\pi^+$ energy distribution was used to infer that the T_{cc}^+ resonance is mostly isospin 0.

The energy difference between the $D^{*0}D^+$ and $D^{*+}D^0$ scattering thresholds is $\delta = 1.41 \pm 0.03$ MeV. The two channels are related by isospin symmetry, which is broken by the energy difference δ. The binding energy of T_{cc}^+ for the $D^{*0}D^+$ channel is $\delta + |\varepsilon_T| = 1.77 \pm 0.05$ MeV. The binding momentum for that channel is $\gamma_{0+} = 58.5 \pm 0.8$ MeV. A simple coupled-channel model defined by wave functions analogous to Eqs. (3) and (10) was used in Refs. [20,22]. We introduce a coupled-channel model defined by wave functions analogous to Eqs. (7) and (11), which have more physical behavior at large momentum. We assume that isospin symmetry requires the wave

functions at the origin in the two channels to be equal, as in Eq. (12). If Λ is varied from $m_\pi/2$ to m_π to $2m_\pi$, the ratio Z_{0+} of the probabilities for the $D^{*0}D^+$ and $D^{*+}D^0$ components from Eq. (13) ranges from 0.34 to 0.38 to 0.41.

III. XEFT FOR THE DOUBLE-CHARM SECTOR

In this section we describe the effective field theory XEFT for low-energy charm mesons and pions, and we give the Feynman rules for XEFT relevant to T_{cc}^+.

A. Effective field theories for charm mesons and pions

The universal wave function in Eq. (2) and the scattering amplitude in Eq. (5) can be derived from a zero-range effective field theory (ZREFT) with a single scattering channel [18]. The simplest single-channel ZREFT has been applied previously to the $X(3872)$ and its constituents $D^{*0}\bar{D}^0$ and $D^0\bar{D}^{*0}$ [18]. Its region of validity extends at most up to the $D^{*+}D^-$ scattering threshold, which is 8.2 MeV above the $D^{*0}\bar{D}^0$ threshold. ZREFT cannot describe accurately the effects of $D^0\bar{D}^0\pi^0$ states, which can be reached by the decay of a constituent D^{*0} or $\bar{D}^{*0}$. An analogous ZREFT can describe $T_{cc}^+(3875)$ and its constituents $D^{*+}D^0$. Its region of validity extends at most up to the $D^{*0}D^+$ scattering threshold, which is 1.4 MeV above the $D^{*+}D^0$ threshold. ZREFT cannot describe accurately the effects of $D^0D^0\pi^+$ or $D^+D^0\pi^0$ states, which can be reached by the decay of a constituent D^{*+}.

Fleming *et al.* developed an effective field theory called XEFT that describes X and its meson constituents with a much larger region of validity [57]. XEFT is a nonrelativistic effective field theory for charm mesons $D^{(*)}$ and $\bar{D}^{(*)}$ and pions π. The states described explicitly by XEFT are $D^*\bar{D}$, $D\bar{D}^*$, $D\bar{D}\pi$, and X with total energy in the region near the $D^*\bar{D}$ thresholds. XEFT can equally well be applied to T_{cc}^+ and its meson constituents. The states described explicitly by XEFT are D^*D, $DD\pi$, and T_{cc}^+ with total energy in the region near the D^*D thresholds.

The region of validity of XEFT is limited by the nonrelativistic approximation for the pion to momenta less than the pion mass m_π. The natural scale for the ultraviolet momentum cutoff Λ of XEFT is therefore m_π. The corresponding scale for the kinetic energy of a pion is m_π. The corresponding scale for the kinetic energy of two charm mesons is m_π^2/M, where M is the charm-meson mass, which is about 10 MeV.

A Galilean-invariant formulation of XEFT that exploits the approximate conservation of mass in the transitions $D^* \leftrightarrow D\pi$ was developed in Ref. [58]. In Galilean-invariant XEFT, the spin-0 charm mesons D^0 and D^+ have the same kinetic mass M and the pions π^0 and π^+ have the same kinetic mass m. Conservation of kinetic mass requires the spin-1 charm mesons D^{*0} and D^{*+} to have the same kinetic mass $M+m$. The difference between the physical mass and the kinetic mass of a particle is taken into account through its rest energy. In XEFT, the number of charm mesons with a charm quark and the number of charm mesons with a charm antiquark are both conserved. In Galilean-invariant XEFT, the pion number defined by the sum of the numbers of D^*, $\bar{D}^*$, and π mesons is also conserved. The conservation of pion number simplifies calculations in XEFT by reducing the number of diagrams. Galilean invariance also simplifies the analytic expressions for loop diagrams. Furthermore, it simplifies the renormalization of XEFT by constraining ultraviolet divergences. An improved formulation of Galilean-invariant XEFT that is particularly convenient for calculations beyond leading order was developed in Ref. [59].

In Ref. [60], Braaten, Hammer, and Mehen pointed out that XEFT could also be applied to sectors with pion number larger than 1. It was applied specifically to the sector with pion number 2 consisting of $D^*\bar{D}^*$, $D^*\bar{D}\pi$, $D\bar{D}^*\pi$, $D\bar{D}\pi\pi$, and $X\pi$ with total energy in the region near the $D^*\bar{D}^*$ thresholds [60]. The states in the pion-number 2 sector with double charm described explicitly by XEFT are D^*D^*, $D^*D\pi$, $DD\pi\pi$, and $T_{cc}^+\pi$ with total energy in the region near the D^*D^* thresholds.

B. Feynman rules

We denote the masses of the spin-0 charm mesons D^0 and D^+ by M_0 and M_+, the masses of the spin-1 charm mesons D^{*0} and D^{*+} by M_{*0} and M_{*+}, and the masses of the pions π^0 and π^+ by m_0 and m_+ (or collectively by m_π). We choose the kinetic mass M of the spin-0 charm mesons to be M_0 and the kinetic mass m of the pions to be m_+. Galilean invariance then requires the kinetic mass of the spin-1 charm mesons to be $M_* = M + m$ and the kinetic mass of T_{cc}^+ to be $M_T = 2M + m$. The Galilean-invariant reduced masses of D^*D and $D\pi$ are $\mu = MM_*/M_T$ and $\mu_\pi = Mm/M_*$. The reduced mass of T_{cc}^+ and a pion is $\mu_{\pi T} = M_T m/(2M_*)$.

We proceed to give the Feynman rules for Galilean-invariant XEFT at leading order (LO) applied to the $DD\pi$ and $DD\pi\pi$ sectors of QCD. Our Feynman rules are essentially those in Ref. [59], in which the geometric series of $D^{*+}D^0$ bubble diagrams have been summed up into a T_{cc}^+ propagator. The Feynman rule for the propagator of D^{*+} with energy E relative to the $D^0\pi^+$ threshold, momentum $\boldsymbol{p}$, and vector indices i and j is

$$\frac{i\delta^{ij}}{E - p^2/(2(M+m)) - \delta_{0+} + i\Gamma_{*+}/2}, \tag{14}$$

where $\delta_{0+} = M_{*+} - M_0 - m_+ = 5.9$ MeV and $\Gamma_{*+} = 83.4 \pm 1.8$ keV is the measured decay width of D^{*+}. The Feynman rule for the complete propagator of T_{cc}^+ with energy E relative to the $D^0D^0\pi^+$ threshold, momentum $\boldsymbol{P}$, and vector indices i and j is

$$\frac{-i\delta^{ij}}{-\gamma_T+\sqrt{-2\mu(E_{\rm cm}-\delta_{0+}+i\Gamma_{*+}/2)}}, \tag{15}$$

where $E_{\rm cm}=E-P^2/[2(2M+m)]$ is the Galilean-invariant combination of E and P. The real binding momentum γ_T is a significant simplification over XEFT applied to X, whose binding momentum γ_X must be complex to take into account short-distance decay channels such as $X\to J/\psi\pi^+\pi^-$. The external-line factor for an outgoing T_{cc}^+ with polarization vector $\boldsymbol{\varepsilon}$ and vector index i is

$$\sqrt{\gamma_T/\mu}\,\varepsilon^{i*}. \tag{16}$$

The vertex connecting $D^{*+}D^0$ lines to the T_{cc}^+ propagator is

$$-i\sqrt{2\pi/\mu}\,\delta^{ij}, \tag{17}$$

where i and j are the vector indices of T_{cc}^+ and D^{*+}. In Ref. [59], the factor $\sqrt{2\pi/\mu}$ was removed from this vertex in favor of multiplying the propagator in Eq. (15) by $2\pi/\mu$ and multiplying the external line factor in Eq. (16) by $\sqrt{2\pi/\mu}$. Because the complete T_{cc}^+ propagator is obtained by summing a geometric series of $D^{*+}D^0$ bubble diagrams, the $D^{*+}D^0$ lines emerging from the vertex in Eq. (17) are not allowed to close into a bubble before some other interaction, such as the emission of a pion.

The Feynman rule for the $D^{*+}\leftrightarrow D^0\pi^+$ vertex in Galilean-invariant XEFT is [58,59]

$$\pm\frac{g}{\sqrt{2m}f_\pi}\frac{(M\boldsymbol{q}-m\boldsymbol{p}_0)^i}{M+m}, \tag{18}$$

where i is the vector index for D^{*+} and $\boldsymbol{q}$ and $\boldsymbol{p}_0$ are the momenta of π^+ and D^0. The overall sign is $+$ if the $D^0\pi^+$ lines are outgoing and $-$ if they are incoming. The Feynman rules for the $D^{*0}\leftrightarrow D^0\pi^0$, $D^{*+}\leftrightarrow D^+\pi^0$, and $D^{*0}\leftrightarrow D^+\pi^-$ vertices differ by the Clebsch-Gordan factors $+1/\sqrt{2}$, $-1/\sqrt{2}$, and $+1$, respectively. In the prefactor in Eq. (18), $f_\pi=130.5$ MeV is the pion decay constant and g is a dimensionless coupling constant that can be determined from the decay width of D^{*+} and its branching fraction into $D^0\pi^+$. Having chosen $m=m_+$, the value of g is given by $g^2=0.329\pm0.008$. In the center-of-momentum (CM) frame defined by $\boldsymbol{p}_0+\boldsymbol{q}=0$, the momentum-dependent factor in Eq. (18) reduces to q^i. In original XEFT, the momentum-dependent factor is q^i in all frames.

A coupled-channel model for a loosely bound molecule with two coupled channels related by a symmetry at short distances was introduced in Sec. II. The wave functions for the two coupled channels in Eqs. (7) and (11) satisfy the symmetry condition in Eq. (12). If an amplitude in XEFT for producing T_{cc}^+ is expressed in a form with a factor of $1/(k^2+\gamma^2)$ from a D^0 propagator, where k is the relative momentum of the constituents D^{*+} and D^0, then the corresponding amplitude in the coupled-channel model can be obtained by making the substitution

$$\frac{1}{k^2+\gamma^2}\to\frac{1}{\sqrt{1+Z_{0+}}}\frac{\sqrt{(\Lambda+\gamma)\Lambda}}{\Lambda-\gamma}\left(\frac{1}{k^2+\gamma^2}-\frac{1}{k^2+\Lambda^2}\right), \tag{19}$$

where $Z_{0+}=(\Lambda+\gamma)\gamma/[(\Lambda+\gamma_{0+})\gamma_{0+}]$ is the relative probability of the $D^{*0}D^+$ channel. This is equivalent to replacing the universal wave function $\psi_T(k)$ by $\psi_T^{(\Lambda)}(k)/\sqrt{1+Z_{0+}}$. If an amplitude for producing T_{cc}^+ through the $D^{*0}D^+$ channel is expressed in a form with Eq. (17) as the $D^{*0}D^+$-to-T_{cc}^+ vertex and with a factor of $1/(k^2+\gamma_{0+}^2)$ from a D^+ propagator, where k is the relative momentum of D^{*0} and D^+, then the amplitude in the coupled-channel model can be obtained by making the substitution

$$\frac{1}{k^2+\gamma_{0+}^2}\to-\frac{1}{\sqrt{1+Z_{0+}}}\frac{\sqrt{(\Lambda+\gamma)\Lambda}}{\Lambda-\gamma_{0+}}\left(\frac{1}{k^2+\gamma_{0+}^2}-\frac{1}{k^2+\Lambda^2}\right). \tag{20}$$

The relative minus sign compared to Eq. (19) comes from the isospin-0 combination $(D^{*+}D^0-D^{*0}D^+)/\sqrt{2}$. The integrals over $\boldsymbol{k}$ of the right sides of Eqs. (19) and (20) differ only by a minus sign. This is consistent with our assumption that isospin symmetry at short distances requires the wave functions at the origin for the channels $D^{*+}D^0$ and $D^{*0}D^+$ to be equal, as in Eq. (12). The ratio of the integrals over $\boldsymbol{k}$ of the squares of the right sides of Eqs. (20) and (19) is equal to the relative probability Z_{0+} of the $D^{*0}D^+$ channel.

IV. PRODUCTION AT A HADRON COLLIDER

In this section we consider the production of $T_{cc}^+(3875)$ at a high-energy hadron collider such as the LHC. We compare various aspects of its production with that of $X(3872)$.

A. Production mechanisms

The production of X at a hadron collider has two contributions that can be resolved experimentally: *bottom hadron decay* and *prompt production*. In bottom hadron decay, a b or $\bar{b}$ is created at the primary vertex for the colliding hadrons. It hadronizes into a bottom hadron, which travels a measurable distance before decaying through the weak interaction at a secondary vertex into a final state that includes X. The decay products of X, such as $J/\psi\pi^+\pi^-$, emerge from that secondary vertex. In the prompt production of X, the $c\bar{c}$ constituents of X are created at the primary vertex by QCD interactions and the decay products of X emerge from the primary vertex.

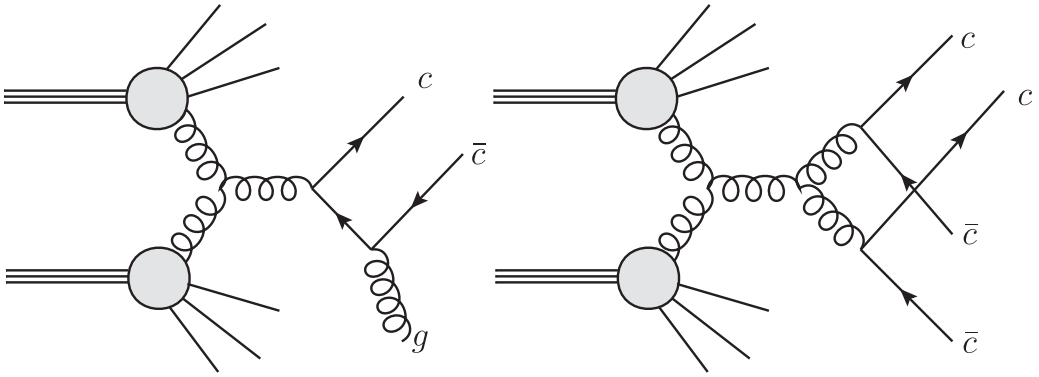

FIG. 1. Feynman diagrams for the prompt production of X (left) and T_{cc}^{+} (right) through SPS.

Bottom hadron decay can be distinguished from prompt production by the distribution of the measured distance between the X decay vertex and the primary collision vertex. In the production of T_{cc}^{+} at a hadron collider, there is no significant production mechanism analogous to bottom hadron decay. The production of T_{cc}^{+} is entirely prompt. Its decay products, such as $D^0D^0\pi^+$, emerge from the primary vertex.

At a hadron collider, there are two distinct mechanisms for the prompt production of X or the production of T_{cc}^{+}: *single-parton scattering* (SPS) and *double-parton scattering* (DPS). In SPS, the $c\bar{c}$ constituents of X and the cc constituents of T_{cc}^{+} are created with small relative momentum by a single gluon-gluon collision. At leading order in the QCD coupling constant α_s, the parton reaction that produces the $c\bar{c}$ constituents of X is $gg \to c\bar{c} + g$, with diagrams like that on the left side of Fig. 1. This reaction, whose cross section is order α_s^3, also produces a gluon jet recoiling against the collinear $c\bar{c}$ pair. At leading order in α_s, the parton reaction that produces the cc constituents of T_{cc}^{+} is $gg \to cc\bar{c}\bar{c}$, with diagrams like that on the right side of Fig. 1. This reaction, whose cross section is order α_s^4, also produces two charm antiquark jets recoiling against the collinear cc. In DPS, the $c\bar{c}$ constituents of X and the cc constituents of T_{cc}^{+} are created with small relative momentum by two separate gluon-gluon collisions, such as $gg \to c\bar{c}$ whose cross section is order α_s^2. The Feynman diagrams for X and T_{cc}^{+} include those on the left and right side of Fig. 2. There is a small probability that the c from one gluon-gluon collision and the $\bar{c}$ or c from the other have small relative momentum, in which case they can become constituents of X or T_{cc}^{+}.

An intermediate step between the creation of a charm quark or charm antiquark and its becoming a constituent of X or T_{cc}^{+} is the hadronization of c or $\bar{c}$ into a charm meson. A $c\bar{c}$ pair created with small relative momentum can hadronize into a pair of charm mesons $D^{(*)}\bar{D}^{(*)}$ with small relative momentum. If the charm mesons are $D^{*0}\bar{D}^{0}$ or $D^{0}\bar{D}^{*0}$, they may bind to form X. Two charm quarks created with small relative momentum can hadronize into two charm mesons $D^{(*)}D^{(*)}$ with small relative momentum. If the charm mesons are $D^{*+}D^{0}$, they may bind to form T_{cc}^{+}.

An alternative intermediate step between the creation of a $c\bar{c}$ pair with small relative momentum and the formation of X is the hadronization of $c\bar{c}$ into a more compact meson that is a component of the wave function of X at short

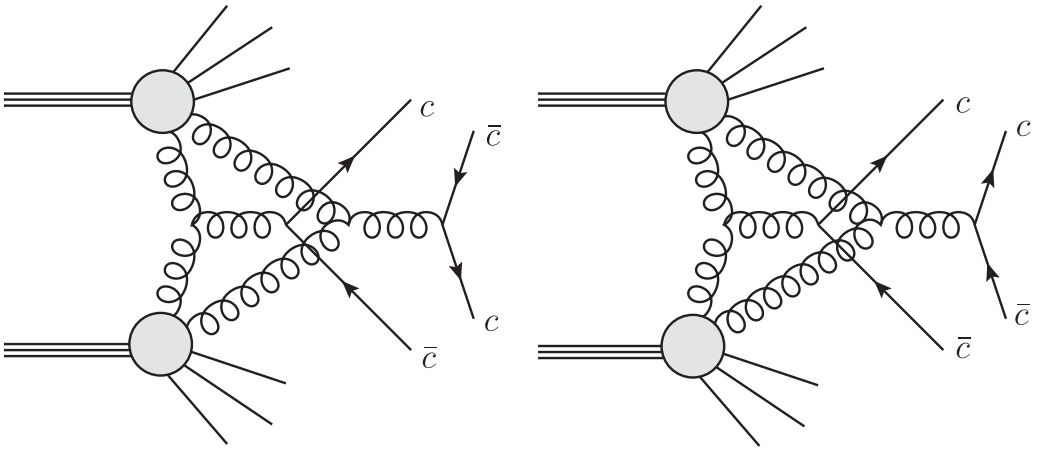

FIG. 2. Feynman diagrams for the prompt production of X (left) and T_{cc}^{+} (right) through DPS.

distances. The X is likely to have a short-distance component that is the $\chi_{c1}(2P)$ charmonium state, whose mass was expected to be less than 100 MeV above the $D^{*0}\bar{D}^0$ threshold. Quantitative calculations of the prompt production rate of X at the LHC through the $\chi_{c1}(2P)$ component of its wave function starting from SPS reactions have been carried out using NRQCD factorization at next-to-leading order [61–63]. The probability for the $\chi_{c1}(2P)$ component of X is a multiplicative factor in the cross section. It can be adjusted to bring the calculated prompt production rate of X into agreement with measurements at the LHC. One cannot, *a priori*, exclude the possibility that X also has a short-distance component that is a compact $c\bar{c}q\bar{q}$ tetraquark meson, although the production rate of X through such a component is much more difficult to quantify. The formulation of the production rate of X entirely in terms of the production of charm mesons does not require its production through $\chi_{c1}(2P)$ or a compact tetraquark state to be ignored. That contribution can be taken into account through the wave function at the origin $\psi_X(r=0)$ of X.

An alternative intermediate step between the creation of cc with small relative momentum and the formation of T_{cc}^+ is the hadronization of cc into a tetraquark meson that is a component of the wave function of T_{cc}^+ at short distances. Such a meson could be a compact $cc\bar{q}\bar{q}$ meson or it could consist of $\bar{q}\bar{q}$ bound to a cc diquark core. The production rate of T_{cc}^+ through such a component would be difficult to quantify. The formulation of the production rate of T_{cc}^+ entirely in terms of the production of charm mesons does not require its production through a more compact tetraquark meson to be ignored. That contribution can be taken into account through the wave function at the origin $\psi_T(r=0)$ of T_{cc}^+.

B. Short-distance production

A charm-meson triangle singularity can be relevant to the production of X or T_{cc}^+ only if the process involves the creation of two charm mesons at points whose separation is much smaller than the radius $\langle r \rangle$ of the loosely bound molecule. There is a significant difference between the SPS and DPS mechanisms in the distance between the points where the charm mesons are created. With the SPS mechanism, the points where the collinear $c\bar{c}$ or cc are created can be localized to within the reciprocals of their transverse momenta to a single point where the gluon-gluon collision occurs. Their subsequent hadronization can produce two charm mesons emerging from that point. With the DPS mechanism, the points where the collinear $c\bar{c}$ or cc are created can be localized to within the reciprocals of their transverse momenta to two separate points where the gluon-gluon collisions occur. Their subsequent hadronization can produce two charm mesons emerging from points separated by a distance comparable to the radius of the proton. Thus the two charm mesons from the SPS mechanism are created at significantly shorter distances than those from the DPS mechanism. However the DPS mechanism may still create charm mesons at short enough distances for a charm-meson triangle singularity to be relevant.

The charm meson $D^{(*)}$ has four spin states (1 for D and 3 for D^*) and three light-flavor states ($\bar{u}$, $\bar{d}$, and $\bar{s}$). Because the available energy in pp collisions at the LHC is so large, a charm quark has approximately equal probabilities to hadronize at short distances into each of the 12 $D^{(*)}$ flavor/spin states. At longer distances, the D^*s all decay into $D\pi$ or $D\gamma$, and the resulting probabilities for D^0, D^+ and D_s^+ are roughly in the proportions 6:2:4. A charm quark and antiquark created with small relative momentum have approximately equal probabilities to hadronize at short distances into each of the 144 $D^{(*)}\bar{D}^{(*)}$ flavor/spin states. Because of the effects of identical bosons, two charm quarks created with small relative momentum have approximately equal probabilities to hadronize at short distances into each of the 78 $D^{(*)}D^{(*)}$ flavor/spin states. For example, the short-distance hadronization probabilities for each of the six spin states of $D^{*+}D^{*+}$ and each of the nine spin states of $D^{*+}D^{*0}$ are approximately equal to those for each of the three light-flavor states D^+D^+, D^+D^0, and D^0D^0. The production rates of two charm mesons with small relative momentum may be modified at longer distances in channels with a resonance near the threshold. The existence of the T_{cc}^+ implies that there is an S-wave resonance near the threshold in the $D^{*+}D^0$ channel.

At a high-energy proton-proton collider like the LHC, the reactions that produce T_{cc}^+ or two charm mesons $D^{(*)}D^{(*)}$ also produce hundreds or even thousands of additional particles. It is convenient to consider the reaction in the CM frame of $D^{(*)}D^{(*)}$. In this frame, the colliding protons and most of the additional particles have very large momenta. If all the additional particles have momenta larger than $q_{\rm max}$ in that frame, the two charm mesons $D^{(*)}D^{(*)}$ are guaranteed to be created at points separated by less than $1/q_{\rm max}$. For reactions involving the charm mesons that involve momenta less than $q_{\rm max}$, they might as well be created at a point. An effective field theory for charm mesons and pions, such as XEFT, can be applied to the short-distance production of $D^{(*)}D^{(*)}$ by introducing local operators that create two charm mesons at a point. The amplitude for producing a given set of final-state particles from the creation of $D^{(*)}D^{(*)}$ at a point can be expressed as a sum of Feynman diagrams whose initial state is the creation of the charm mesons at a point with a vertex $\mathcal{A}_{D^{(*)}D^{(*)}}$ determined by the local operator. The vertices $\mathcal{A}_{D^{(*)}D^{(*)}}$ must be such that the short-distance production rates for each of the 78 $D^{(*)}D^{(*)}$ flavor/spin states are approximately equal.

A local operator can create particles with arbitrarily large energies. In an effective field theory, the inclusive production rate from a local operator that creates two charm mesons is ultraviolet divergent and it therefore requires

regularization. A possible ultraviolet cutoff is an upper limit $q_{\max}$ on the momenta of particles in the CM frame of the two charm mesons. Renormalization may require the vertices $\mathcal{A}_{D^{(*)}D^{(*)}}$ to depend on $q_{\max}$. If the effective field theory is XEFT, its results for all production amplitudes can be accurate only if $q_{\max}$ is at most of order m_π. If the effective field theory is Galilean-invariant XEFT, the particles that can be produced by the local operator are strongly constrained by the conservation of charm-quark number and pion number. A vertex of the form $\mathcal{A}_{DD}$, $\mathcal{A}_{D^*D}$, or $\mathcal{A}_{D^*D^*}$ produces final states with pion number 0, 1, or 2, respectively. A final state with pion number 1 or 2 can consist of a pion with large relative momentum and a recoiling system with pion number lower by 1. The recoiling system can be created by a vertex of the form $\mathcal{A}_{DD}$ or $\mathcal{A}_{D^*D}$. Final states that include a pion with relative momentum $q < q_{\max}$ are described explicitly in the effective field theory. The effects of pions with $q > q_{\max}$ can be taken into account through the dependence on $q_{\max}$ of vertices of the form $\mathcal{A}_{DD}$ and $\mathcal{A}_{D^*D}$. Vertices of the form $\mathcal{A}_{D^*D^*}$ do not acquire any dependence on $q_{\max}$ from the interactions of Galilean invariant XEFT.

It has been argued that the prompt production rates of X at the Tevatron and the LHC are orders of magnitude too large for a charm-meson molecule [64]. The argument is based on the assumption that an order-of-magnitude estimate of the production rate of a molecule is the production rate of its constituents with relative momentum less than its binding momentum γ. The production rate of a molecule whose constituents are produced at short distances is actually proportional to the square $|\psi(r=0)|^2$ of its wave function at the origin [65]. For a generic molecule, $|\psi(r=0)|^2$ can be expressed as Λ^3 for some momentum scale Λ of order γ. The production rate of the molecule can therefore be approximated by the production rate of its constituents with relative momentum less than Λ. Since the production rate of the constituents scales as Λ^3, this gives at best an order-of-magnitude estimate of the production rate of the molecule. This estimate does not apply to a loosely bound S-wave molecule, because the universal wave function in Eq. (2) is ultraviolet divergent at the origin. In this case, $|\psi(r=0)|^2$ can be expressed as $\Lambda^2\gamma$ for some momentum scale Λ much larger than γ. The production rate of a loosely bound S-wave molecule can therefore be approximated by the production rate of its constituents with relative momentum less than $(\Lambda^2\gamma)^{1/3}$. If Λ is taken to be of order m_π, the resulting order-of-magnitude estimates for the prompt production rates of X are compatible with the observed production rates at the Tevatron and the LHC [65–67].

C. Multiplicity dependence

The total number of light hadrons in the final state is the multiplicity. At the LHC, the total multiplicity of an event is often in the thousands. An additional hard-parton scattering can increase the multiplicity. The multiplicities of X or T_{cc}^+ events produced by DPS are therefore expected to be larger than those produced by SPS. An additional jet produced by a hard scattering can increase the multiplicity. The multiplicities of T_{cc}^+ events produced by SPS are therefore expected to be larger than those for X events produced by SPS. However, the increase in the multiplicity from an additional hard scattering or from an additional jet are probably small compared to the total multiplicity. The dominant effect of the multiplicity on the production rate for X or T_{cc}^+ could be through the environment a charm meson or a loosely bound charm-meson molecule must propagate through after it is produced. One possible effect of a higher multiplicity is a higher probability for particles produced by a hard scattering to interact with comoving partons or hadrons. Esposito *et al.* have considered the effects on the production of X from its breakup by collisions with comovers and from its formation through recombination reactions involving comovers [68]. Once a loosely bound charm-meson molecule has formed, almost any interaction with a comover will break it up. It is possible that the formation of the molecule from the two charm mesons created by DPS occur most often after they have traveled beyond the reach of comovers. In this case, its production by DPS would be less suppressed by interactions with comovers than its production by SPS.

The LHCb Collaboration has studied the multiplicity dependence of the prompt production of X and $\psi(2S)$ and their production from bottom hadron decays [69]. They measured the yields as functions of the number of charged tracks N_{tracks} in the vertex detector, which has a range of several units of rapidity. The prompt fraction of X decreases with N_{tracks} from about 94% in the lowest bin near $N_{\text{tracks}} = 30$ to about 71% in the highest bin near 120. The decreasing prompt fraction suggests that the prompt production of X may be dominated by SPS. A theoretical analysis by Esposito *et al.* showed that the prediction of the comover interaction model for the multiplicity dependence of the X-to-$\psi(2S)$ ratio is in good agreement with the LHCb data if X has a size consistent with a compact tetraquark [68]. They used a coalescence model that takes into account the recombination of charm-meson pairs to calculate the multiplicity dependence of the production of X if it is a molecule. Their result for the X-to-$\psi(2S)$ ratio is a rapidly increasing function of N_{tracks}. The analysis in Ref. [70] showed that a good fit to all the LHCb data on the multiplicity dependence of the production of X and $\psi(2S)$ can be obtained if the break-up cross section of X with comoving pions is roughly 3 mb. This value is plausible, given that the break-up cross section for a loosely bound charm-meson molecule should be approximately equal to the cross section for scattering from a charm-meson constituent.

The LHCb Collaboration has also studied the multiplicity dependence of the inclusive production of T_{cc}^+ [10].

The ratio of the yield of T_{cc}^+ in the decay channel $D^0D^0\pi^+$ to the yield of $D^0\bar{D}^0$ seems to be about two or three times larger at values of $N_{\rm tracks}$ greater than about 80 than at smaller values of $N_{\rm tracks}$. It is possible that the increased yield at larger $N_{\rm tracks}$ arises from the DPS mechanism. In this case, the restriction to $N_{\rm tracks} < 80$ could produce a sample of T_{cc}^+ events in which a larger fraction is produced by the SPS mechanism.

V. PRODUCTION OF TWO CHARM MESONS

In this section we consider the production of two spin-1 charm mesons D^*D^* without any accompanying soft pions. Our treatment is similar to that for the prompt production of $D^*\bar{D}^*$ in Ref. [46], but there are additional complications associated with identical bosons.

A. Distinguishable charm mesons

We consider the production of two charm mesons $D^{(*)}D^{(*)}$ plus additional particles y that all have large momenta in the $D^{(*)}D^{(*)}$ CM frame. The short-distance amplitude for creating D^*D^* is represented in XEFT by the vertex in Fig. 3, in which the solid + dashed lines of the D^*s emerge from a point. The amplitudes for creating D^*D and DD can be represented by analogous Feynman diagrams with a solid line for a D. A spin-0 charm meson is described by a scalar field D. A spin-1 charm mesons is described by a vector field D^{*i} with vector index $i = 1, 2, 3$. We denote the short-distance vertex factor for creating DD at a point with small relative momentum while producing additional particles y with large momentum in the DD CM frame by $i\mathcal{A}_{DD+y}$. We denote the analogous short-distance vertex factor for creating D^*D at a point by $i\mathcal{A}^i_{D^*D+y}$. We denote the analogous short-distance vertex factor for creating D^*D^* at a point by $i\mathcal{A}^{ij}_{D^*D^*+y}$. If the two D^*s have the same light flavor, then $\mathcal{A}^{ij}_{D^*D^*+y}$ is symmetric in the indices i and j. We take the relative momentum $\boldsymbol{k}$ of the charm mesons in their CM frame to be smaller than some ultraviolet cutoff $q_{\rm max}$ of order m_π. Since the momenta of all the additional particles y in that frame are larger than $q_{\rm max}$, we take the limit $\boldsymbol{k} \to 0$ in the short-distance vertex factors.

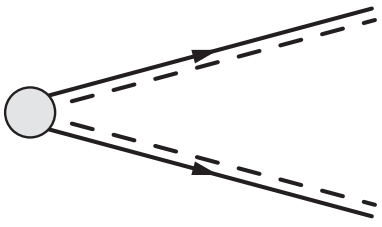

FIG. 3. Feynman diagram in XEFT for the production of D^*D^* from their creation at a point. A D^* is represented by a double (solid + dashed) line with an arrow.

We first consider the short-distance production of the two distinguishable spin-1 charm mesons $D^{*+}D^{*0}$. Under the assumption that there is no resonance near threshold in that channel, the matrix element for producing the final state $D^{*+}D^{*0} + y$ is obtained by contracting the short-distance amplitude $\mathcal{A}^{ij}_{D^{*+}D^{*0}+y}$ with the polarization vectors ε^{i*} and ε'^{j*} for the D^*s. The inclusive differential cross section for producing $D^{*+}D^{*0}$ with relative momentum $\boldsymbol{k}$ in their CM frame can be expressed as

$$d\sigma[D^{*+}D^{*0}] = \sum_{D^* \text{ spins}} \langle \mathcal{A}^{ij}_{D^{*+}D^{*0}} (\mathcal{A}^{kl}_{D^{*+}D^{*0}})^* \rangle \times (\varepsilon^i \varepsilon'^j)^* (\varepsilon^k \varepsilon'^l) \frac{d^3k}{(2\pi)^3 M_*}. \quad (21)$$

The factor in angular brackets involves only short distances,

$$\langle \mathcal{A}^{ij}_{D^{*+}D^{*0}} (\mathcal{A}^{kl}_{D^{*+}D^{*0}})^* \rangle \equiv \frac{1}{\text{flux}} \sum_y \int d\Phi_{(D^*D^*)+y} \times \mathcal{A}^{ij}_{D^{*+}D^{*0}+y} (\mathcal{A}^{kl}_{D^{*+}D^{*0}+y})^*. \quad (22)$$

The product of the short-distance amplitude and its complex conjugate is integrated over the relativistic differential phase space $d\Phi_{(D^*D^*)+y}$ for the additional particles y plus a composite particle with mass $2M_*$ denoted by (D^*D^*), summed over the additional particles y (including their spins), and multiplied by the flux factor 1/flux for the colliding protons. The differential phase space for D^*D^* has been expressed as the product of $d^3P/[(2\pi)^3 2P_0]$ for the composite particle (D^*D^*), which is included in $d\Phi_{(D^*D^*)+y}$, and $d^3k/[(2\pi)^3 M_*]$, where M_* is twice the D^*D^* reduced mass.

We next consider the short-distance production of the two distinguishable spin-0 charm mesons D^+D^0. Under the assumption that there is no resonance near threshold in that channel, the matrix element for producing D^+D^0 plus additional particles y is just the short-distance amplitude $\mathcal{A}_{D^+D^0+y}$. The inclusive differential cross section for producing D^+D^0 with relative momentum $\boldsymbol{k}$ in their CM frame can be expressed as

$$d\sigma[D^+D^0] = \langle \mathcal{A}_{D^+D^0} (\mathcal{A}_{D^+D^0})^* \rangle \frac{d^3k}{(2\pi)^3 M}. \quad (23)$$

The factor in angular brackets involves only short distances:

$$\langle \mathcal{A}_{D^+D^0} (\mathcal{A}_{D^+D^0})^* \rangle \equiv \frac{1}{\text{flux}} \sum_y \int d\Phi_{(DD)+y} \times \mathcal{A}_{D^+D^0+y} (\mathcal{A}_{D^+D^0+y})^*. \quad (24)$$

The product of the short-distance amplitude and its complex conjugate is integrated over the relativistic differential phase space $d\Phi_{(DD)+y}$ for the additional particles y plus a composite particle with mass $2M$ denoted by (DD). The cross section in Eq. (23) is for the production of D^+D^0 at short distances. It does not include the feed down from the production of D^*D^* or D^*D at short distances followed by decays $D^* \to D\pi, D\gamma$.

In the CM frame of $D^{*+}D^{*0}$, the short-distance amplitude $\mathcal{A}^{ij}_{D^{*+}D^{*0}+y}$ is a Cartesian tensor with vector indices ij. The indices ij can be carried by the metric tensor δ^{ij}, by momentum vectors of additional particles y or the colliding protons, or by polarization vectors, spinors, or tensors associated with their spins. The indices ij cannot be carried by the relative momentum vector $\boldsymbol{k}$ of the two D^*s, because the limit $\boldsymbol{k} \to 0$ has been taken in the short-distance amplitude. The weighted average $\langle \mathcal{A}^{ij}_{D^{*+}D^{*0}} (\mathcal{A}^{kl}_{D^{*+}D^{*0}})^* \rangle$ of the product of short-distance amplitudes in Eq. (22) is a Cartesian tensor with vector indices $ijkl$. The indices cannot be carried by the momentum vector of any of the additional particles y, because they have been integrated over. They cannot be carried by the polarization vector, spinor, or tensor associated with one of their spins, because the spins have been summed over. The indices can however be carried by the momentum vector of one of the colliding protons or by its polarization spinor. That possibility can be removed by averaging over the spins of the colliding protons and by averaging over the directions of their momenta in the CM frame of the two charm mesons. Averaging over the directions of the proton momenta in the charm-meson CM frame has the same effect as averaging over the directions of the total momentum $\boldsymbol{P}$ of the charm mesons in the pp CM frame. From now on, it will be understood that the weighted average of an amplitude and its complex conjugate, such as that in Eq. (22) or Eq. (24), is also averaged over the spins of the colliding protons and averaged over the directions of their momenta in the CM frame of the two charm mesons. The weighted average in Eq. (22) must then be a linear combination of $\delta^{ik}\delta^{jl}$, $\delta^{il}\delta^{jk}$, and $\delta^{ij}\delta^{kl}$. The condition that the 78 flavor/spin states of $D^{(*)}D^{(*)}$ are produced equally often at short distances can be implemented by keeping only the $\delta^{ik}\delta^{jl}$ term. The weighted average in Eq. (22) can be related to the weighted average in Eq. (24). Since the difference between the masses $2M_*$ and $2M$ of the composite particles (D^*D^*) and (DD) in the phase-space integrals in Eq. (22) and Eq. (24) is tiny compared to the collision energy, it can be ignored. The resulting relation between the weighted averages has the form

$$\langle \mathcal{A}^{ij}_{D^{*+}D^{*0}} (\mathcal{A}^{kl}_{D^{*+}D^{*0}})^* \rangle = \langle \mathcal{A}_{D^+D^0} (\mathcal{A}_{D^+D^0})^* \rangle \delta^{ik}\delta^{jl}. \quad (25)$$

After multiplying by the polarization vectors in Eq. (21) and summing over the spin states of $D^{*+}D^{*0}$, we obtain

$$\sum_{D^* \text{ spins}} \langle \mathcal{A}^{ij}_{D^{*+}D^{*0}} (\mathcal{A}^{kl}_{D^{*+}D^{*0}})^* \rangle (\varepsilon^i \varepsilon'^j)^* (\varepsilon^k \varepsilon'^l) = 9 \langle \mathcal{A}_{D^+D^0} (\mathcal{A}_{D^+D^0})^* \rangle. \quad (26)$$

The prefactor in Eq. (25) was chosen so the prefactor in Eq. (26) is the number of $D^{*+}D^{*0}$ spin states.

Our final result for the $D^{*+}D^{*0}$ cross section is obtained by inserting Eq. (26) into Eq. (21),

$$d\sigma[D^{*+}D^{*0}] = 9 \langle \mathcal{A}_{D^+D^0} (\mathcal{A}_{D^+D^0})^* \rangle \frac{d^3k}{(2\pi)^3 M_*}. \quad (27)$$

The differential cross section $d\sigma/d^3k$ for $D^{*+}D^{*0}$ differs from that for D^+D^0 from Eq. (23) by the spin factor 9 and the mass ratio M/M_*.

B. Identical charm mesons

We next consider the short-distance production of the two identical spin-1 charm mesons $D^{*+}D^{*+}$. Under the assumption that there is no resonance near threshold in that channel, the matrix element for producing the final state $D^{*+}D^{*+} + y$ is obtained by contracting the short-distance amplitude $\mathcal{A}^{ij}_{D^{*+}D^{*+}+y}$ with the polarization vectors ε^{i*} and ε'^{j*} for the D^*s. The inclusive differential cross section for producing $D^{*+}D^{*+}$ with relative momentum $\boldsymbol{k}$ in their CM frame can be expressed as

$$d\sigma[D^{*+}D^{*+}] = \frac{1}{2} \sum_{D^* \text{ spins}} \langle \mathcal{A}^{ij}_{D^{*+}D^{*+}} (\mathcal{A}^{kl}_{D^{*+}D^{*+}})^* \rangle \times (\varepsilon^i \varepsilon'^j)^* (\varepsilon^k \varepsilon'^l) \frac{d^3k}{(2\pi)^3 M_*}. \quad (28)$$

The short-distance factor is defined by a weighted average analogous to that in Eq. (22). The prefactor of $1/2$ in Eq. (28) compensates for overcounting the states of the identical bosons $D^{*+}D^{*+}$.

We next consider the short-distance production of the two identical spin-0 charm mesons D^+D^+. Under the assumption that there is no resonance near threshold in that channel, the matrix element for producing D^+D^+ plus additional particles y is just the short-distance amplitude $\mathcal{A}_{D^+D^+ + y}$. The inclusive differential cross section for producing D^+D^+ with relative momentum $\boldsymbol{k}$ in their CM frame can be expressed as

$$d\sigma[D^+D^+] = \frac{1}{2} \langle \mathcal{A}_{D^+D^+} (\mathcal{A}_{D^+D^+})^* \rangle \frac{d^3k}{(2\pi)^3 M}. \quad (29)$$

The short-distance factor is defined by a weighted average analogous to that in Eq. (24). The prefactor of $1/2$ in Eq. (29) compensates for overcounting the states of the identical bosons D^+D^+. The cross section in Eq. (29) is for the production of D^+D^+ at short distances. It does not

include the feed down from the production of D^*D^* or D^*D at short distances followed by decays $D^* \to D\pi, D\gamma$.

In the CM frame of $D^{*+}D^{*+}$, the short-distance amplitude $\mathcal{A}^{ij}_{D^{*+}D^{*+}+y}$ is a Cartesian tensor with vector indices ij. The weighted average $\langle \mathcal{A}^{ij}_{D^{*+}D^{*+}} (\mathcal{A}^{kl}_{D^{*+}D^{*+}})^* \rangle$ analogous to that in Eq. (22) is a Cartesian tensor with vector indices $ijkl$ that can only be carried by the metric tensor. Because the $D^{*+}D^{*+}$ are identical bosons, the indices must be symmetric under interchange of i and j and under interchange of k and l. It must therefore be a linear combination of $\delta^{ik}\delta^{jl} + \delta^{il}\delta^{jk}$ and $\delta^{ij}\delta^{kl}$. The condition that the 78 flavor/spin states of $D^{(*)}D^{(*)}$ are produced equally often at short distances can be implemented by keeping only the $\delta^{ik}\delta^{jl} + \delta^{il}\delta^{jk}$ term. The weighted average in Eq. (28) can be related to the weighted average in Eq. (29),

$$\langle \mathcal{A}^{ij}_{D^{*+}D^{*+}} (\mathcal{A}^{kl}_{D^{*+}D^{*+}})^* \rangle = \frac{1}{2} \langle \mathcal{A}_{D^+D^+} (\mathcal{A}_{D^+D^+})^* \rangle \times (\delta^{ik}\delta^{jl} + \delta^{il}\delta^{jk}). \tag{30}$$

After multiplying by the polarization vectors in Eq. (28) and summing over the spin states of $D^{*+}D^{*+}$, we obtain

$$\sum_{D^* \text{ spins}} \langle \mathcal{A}^{ij}_{D^{*+}D^{*+}} (\mathcal{A}^{kl}_{D^{*+}D^{*+}})^* \rangle (\varepsilon^i \varepsilon'^j)^* (\varepsilon^k \varepsilon'^l) = 6 \langle \mathcal{A}_{D^+D^+} (\mathcal{A}_{D^+D^+})^* \rangle. \tag{31}$$

The prefactor in Eq. (30) was chosen so the prefactor in Eq. (31) is the number of $D^{*+}D^{*+}$ spin states.

Our final result for the $D^{*+}D^{*+}$ cross section is obtained by inserting Eq. (31) into Eq. (28),

$$d\sigma[D^{*+}D^{*+}] = 6 \langle \mathcal{A}_{D^+D^+} (\mathcal{A}_{D^+D^+})^* \rangle \frac{d^3k}{2(2\pi)^3 M_*}. \tag{32}$$

The differential cross section $d\sigma/d^3k$ for $D^{*+}D^{*+}$ differs from that for D^+D^+ from Eq. (29) by the spin factor 6 and the mass ratio M/M_*.

The short-distance cross sections for the two identical bosons D^+D^+ in Eq. (29) and the two distinguishable bosons D^+D^0 in Eq. (23) must be equal. The short-distance factors in those cross sections must therefore differ by a factor of 2,

$$\langle \mathcal{A}_{D^+D^+} (\mathcal{A}_{D^+D^+})^* \rangle = 2 \langle \mathcal{A}_{D^+D^0} (\mathcal{A}_{D^+D^0})^* \rangle. \tag{33}$$

The cross sections for the two identical bosons $D^{*+}D^{*+}$ in Eq. (32) and the two distinguishable bosons $D^{*+}D^{*0}$ in Eq. (27) therefore differ by the ratio $2/3$ of the numbers of their spin states.

VI. PRODUCTION OF $D^{*+}D^0$ AND T_{cc}^+

In this section, we consider the production of $D^{*+}D^0$ and T_{cc}^+ without any accompanying soft pions. Our treatment is similar to that for the prompt production of $D^{*0}\bar{D}^0$, $D^0\bar{D}^{*0}$, and X in Ref. [46]. The results are consistent with factorization formulas first derived in Ref. [71].

A. Production of $D^{*+}D^0$

The existence of T_{cc}^+ implies that there is an S-wave resonance near threshold in the $D^{*+}D^0$ channel. The resonance must be taken into account in the production of $D^{*+}D^0$ with small relative momentum as well as in the production of T_{cc}^+. We first consider the production of $D^{*+}D^0$. The two Feynman diagrams in XEFT for the production of $D^{*+}D^0$ by their creation at a point are shown in Fig. 4. The blob on the left side of each diagram is the vertex $i\mathcal{A}^i_{D^{*+}D^0+y}$ for creating the charm mesons at a point while producing additional particles y with large momenta in the $D^{*+}D^0$ CM frame. The first diagram in Fig. 4 is the tree amplitude for producing $D^{*+}D^0$ without any subsequent interaction between the charm mesons. The second diagram in Fig. 4 is the loop amplitude for producing $D^{*+}D^0$ with one or more subsequent rescatterings of the charm mesons. These rescattering amplitudes form a geometric series that can be summed up in terms of the complete propagator for T_{cc}^+ in Eq. (15). We take the relative momenta of the charm mesons in their CM frame to be $\boldsymbol{\ell}$ for the $D^{*+}D^0$ that are created and $\boldsymbol{k}$ for the final-state $D^{*+}D^0$. The loop integral over $\boldsymbol{\ell}$ should be evaluated at a total energy $E = \delta_{0+} - i\Gamma_{*+}/2 + k^2/(2\mu)$ given by the sum of the complex energy of the D^{*+} and the real energy

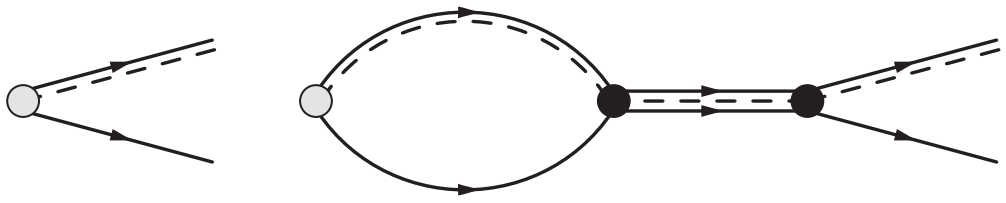

FIG. 4. Feynman diagrams in XEFT for the production of $D^{*+}D^0$ from the creation of the charm mesons at a point. A D^0 is represented by a solid line with an arrow. The T_{cc}^+ is represented by a triple (solid + dashed + solid) line.

of the D^0. The resulting expression for the sum of the two diagrams is

$$\mathcal{A}_{D^{*+}D^0+y}(\boldsymbol{k}) = \mathcal{A}^i_{D^{*+}D^0+y}\left(1+\frac{4\pi}{-\gamma_T-ik}\right.$$
$$\left.\times\int\frac{d^3\ell}{(2\pi)^3}\frac{1}{\ell^2-(k^2+i\epsilon)}\right)\varepsilon^{i*}, \quad (34)$$

where $\gamma_T=\sqrt{2\mu|\varepsilon_T|}$. The ultraviolet-divergent loop integral can be evaluated analytically after imposing a sharp ultraviolet cutoff $|\boldsymbol{\ell}|<(\pi/2)\Lambda$ on the loop momentum. The amplitude for producing $D^{*+}D^0$ with polarization vector $\boldsymbol{\varepsilon}$ for the D^{*+} is

$$\mathcal{A}_{D^{*+}D^0+y}(\boldsymbol{k}) = \mathcal{A}^i_{D^{*+}D^0+y}\frac{\Lambda-\gamma_T}{-\gamma_T-ik}\varepsilon^{i*}. \quad (35)$$

The factor $\Lambda-\gamma_T$ in the numerator can be expressed as $\sqrt{2\pi/\gamma_T}\psi_T(r=0)$, where $\psi_T(r=0)$ is the universal wave function at the origin for T^+_{cc} given by Eq. (4) with $\gamma=\gamma_T$.

The inclusive differential cross section for producing $D^{*+}D^0$ with small relative momentum $\boldsymbol{k}$ in their CM frame can be expressed as

$$d\sigma[D^{*+}D^0] = \frac{1}{\text{flux}}\sum_{D^*\text{ spins}}\sum_y\int d\Phi_{(D^*D)+y}$$
$$\times|\mathcal{A}_{D^{*+}D^0+y}(\boldsymbol{k})|^2\frac{d^3k}{(2\pi)^3 2\mu}, \quad (36)$$

where $d\Phi_{(D^*D)+y}$ is the relativistic differential phase space for all the additional particles y plus a composite particle denoted by (D^*D) with mass M_*+M. The relativistic differential phase space for $D^{*+}D^0$ has been expressed as the product of the differential phase space $d^3P/[(2\pi)^3 2P_0]$ for the composite particle (D^*D) and $d^3k/[(2\pi)^3 2\mu]$, where μ is the D^*D reduced mass. The cross section in Eq. (36) does not include the feed down from the production of D^*D^* at short distances followed by decays $D^*\to D\pi, D\gamma$.

In the CM frame of $D^{*+}D^0$, the amplitude $\mathcal{A}^i_{D^{*+}D^0+y}$ is a Cartesian vector with index i. The weighted average $\langle\mathcal{A}^i_{D^{*+}D^0}(\mathcal{A}^j_{D^{*+}D^0})^*\rangle$ of the product of amplitudes can be defined as in Eq. (22), except that the composite particle is (D^*D) with mass M_*+M. The weighted average is a Cartesian tensor whose vector indices ij can only be carried by the metric tensor δ^{ij}. This weighted average can be related to the corresponding weighted average $\langle\mathcal{A}_{D^+D^0}(\mathcal{A}_{D^+D^0})^*\rangle$ for two spin-0 charm mesons. Since the difference between the masses M_*+M and $2M$ of the composite particles (D^*D) and (DD) in the phase-space integrals in Eqs. (23) and (36) is tiny compared to the collision energy, it can be ignored. After multiplying the weighted average $\langle\mathcal{A}^i_{D^{*+}D^0}(\mathcal{A}^j_{D^{*+}D^0})^*\rangle$ by the polarization vectors for D^{*+} and summing over its spin states, we obtain

$$\sum_{D^{*+}\text{ spins}}\langle\mathcal{A}^i_{D^{*+}D^0}(\mathcal{A}^j_{D^{*+}D^0})^*\rangle\varepsilon^{i*}\varepsilon^j = 3\langle\mathcal{A}_{D^+D^0}(\mathcal{A}_{D^+D^0})^*\rangle. \quad (37)$$

The prefactor is the number of D^{*+} spin states.

After inserting the amplitude in Eq. (35) into Eq. (36) and then using Eq. (37), the inclusive differential cross section for producing $D^{*+}D^0$ with small relative momentum $\boldsymbol{k}$ in their CM frame reduces to

$$d\sigma[D^{*+}D^0] = 3\langle\mathcal{A}_{D^+D^0}(\mathcal{A}_{D^+D^0})^*\rangle$$
$$\times|\psi_T(r=0)|^2\frac{2\pi/\gamma_T}{k^2+\gamma_T^2}\frac{d^3k}{(2\pi)^3 2\mu}. \quad (38)$$

B. Production of T^+_{cc}

We now turn to the production of T^+_{cc}. The Feynman diagram in XEFT for the production of T^+_{cc} from the creation of $D^{*+}D^0$ at a point is shown in Fig. 5. The blob on the left side of the diagram is the vertex $i\mathcal{A}^i_{D^{*+}D^0+y}$ for creating the charm mesons at a point while producing additional particles y with large momenta in the $D^{*+}D^0$ CM frame. The loop integral should be evaluated at the complex pole energy of T^+_{cc}. In XEFT at LO, the imaginary part of its pole energy is $-\Gamma_{*+}/2$. The complex pole energy of T^+_{cc} in its rest frame relative to the $D^0D^0\pi^+$ threshold is therefore $\delta_{0+}+\varepsilon_T-i\Gamma_{*+}/2$. Upon evaluating the loop integral at this complex energy, the amplitude for producing T^+_{cc} with polarization vector $\boldsymbol{\varepsilon}$ is

$$\mathcal{A}_{T^+_{cc}+y} = -(\mathcal{A}^i_{D^{*+}D^0+y}\sqrt{M_T/2M_*M})\sqrt{8\pi\gamma_T}\varepsilon^{i*}$$
$$\times\int\frac{d^3\ell}{(2\pi)^3}\frac{1}{\ell^2-2\mu(\varepsilon_T+i\epsilon)}. \quad (39)$$

The factor $\sqrt{M_T/2M_*M}$ takes into account the difference between relativistic and nonrelativistic normalizations of states. The ultraviolet-divergent loop integral can be evaluated analytically after imposing a sharp ultraviolet cutoff $|\boldsymbol{\ell}|<(\pi/2)\Lambda$,

$$\mathcal{A}_{T^+_{cc}+y} = -(\mathcal{A}^i_{D^{*+}D^0+y}\sqrt{M_T/2M_*M})\psi_T(r=0)\varepsilon^{i*}, \quad (40)$$

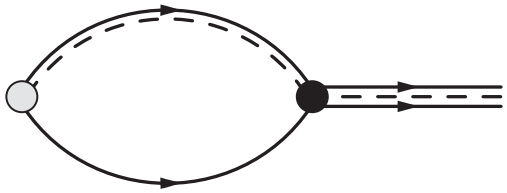

FIG. 5. Feynman diagram in XEFT for the production of T^+_{cc} from the creation of $D^{*+}D^0$ at a point.

where $\psi_T(r=0)$ is the wave function at the origin in Eq. (4) with $\gamma=\gamma_T$.

The inclusive cross section for producing T_{cc}^+ from the creation of $D^{*+}D^0$ at short distances can be expressed as

$$\sigma[T_{cc}^+,\text{no}\,\pi]=\frac{1}{\text{flux}}\sum_{T_{cc}^+\,\text{spins}}\sum_y\int d\Phi_{(D^*D)+y}|\mathcal{A}_{T_{cc}^++y}|^2. \quad (41)$$

We have denoted this cross section by $\sigma[T_{cc}^+,\text{no}\,\pi]$ to emphasize that it is the cross section for producing T_{cc}^+ without any pion with momentum less than the ultraviolet cutoff $q_{\max}$ used to define the short-distance vertices. After inserting the expression for the amplitude in Eq. (40) and then using Eq. (37), the cross section for T_{cc}^+ reduces to

$$\sigma[T_{cc}^+,\text{no}\,\pi]=\langle\mathcal{A}_{D^+D^0}(\mathcal{A}_{D^+D^0})^*\rangle\frac{3}{2\mu}|\psi_T(r=0)|^2. \quad (42)$$

The short-distance factor in angular brackets in the cross section for T_{cc}^+ in Eq. (42) is the same as that in the differential cross section for producing $D^{*+}D^0$ in Eq. (38). Those short-distance factors can therefore be eliminated to get a relation between the cross sections. The factors of $|\psi_T(r=0)|^2$ are also eliminated in that relation. The invariant kinetic energy of $D^{*+}D^0$ is its total kinetic energy $E=k^2/(2\mu)$ in the $D^{*+}D^0$ CM frame. The cross section for $D^{*+}D^0$ differential in E is

$$\frac{d\sigma}{dE}[D^{*+}D^0]=\sigma[T_{cc}^+,\text{no}\,\pi]\frac{\mu/(\pi\gamma_T)}{2\mu E+\gamma_T^2}(2\mu E)^{1/2}. \quad (43)$$

Note that $\sigma[T_{cc}^+,\text{no}\,\pi]$ has a factor of γ_T that cancels the explicit factor of $1/\gamma_T$. This relation between the cross sections is consistent with the imaginary part of the universal scattering amplitude in Eq. (6).

The T_{cc}^+ can also be produced from the creation of $D^{*0}D^+$ at short distances, with the subsequent formation of T_{cc}^+ proceeding through the $D^{*0}D^+$ component of its wave function. This contribution can be taken into account in the coupled-channel model introduced in Sec. II, which can be implemented by using the prescriptions in Eqs. (19) and (20). The amplitudes for producing T_{cc}^+ through its $D^{*+}D^0$ and $D^{*0}D^+$ components have different short-distance factors $\mathcal{A}^i_{D^{*+}D^0+y}$ and $\mathcal{A}^i_{D^{*0}D^++y}$. The cross section therefore has interference terms with the short-distance factors $\langle\mathcal{A}^i_{D^{*+}D^0}(\mathcal{A}^j_{D^{*0}D^+})^*\rangle$ and $\langle\mathcal{A}^i_{D^{*0}D^+}(\mathcal{A}^j_{D^{*+}D^0})^*\rangle$. They are suppressed by the random phases in the sum over the many additional particles y. The terms with short-distance factors $\langle\mathcal{A}^i_{D^{*+}D^0}(\mathcal{A}^j_{D^{*+}D^0})^*\rangle$ and $\langle\mathcal{A}^i_{D^{*0}D^+}(\mathcal{A}^j_{D^{*0}D^+})^*\rangle$ are not suppressed, because they are sums of positive quantities. The contribution to the T_{cc}^+ cross section from its $D^{*+}D^0$ and $D^{*0}D^+$ components can be obtained by replacing $|\psi_T(r=0)|^2$ in Eq. (42) by $|\psi_T^{(\Lambda)}(r=0)|^2/(1+Z_{0+})$ and $|\psi_{0+}^{(\Lambda)}(r=0)|^2/(1+Z_{0+})$, respectively. Isospin symmetry at short distances implies that these two contributions are equal. The total cross section in the coupled-channel model for producing T_{cc}^+ without an accompanying soft pion is therefore

$$\sigma^{(\Lambda)}[T_{cc}^+,\text{no}\,\pi]=\langle\mathcal{A}_{D^+D^0}(\mathcal{A}_{D^+D^0})^*\rangle\frac{3}{(1+Z_{0+})\mu}\times|\psi_T^{(\Lambda)}(r=0)|^2. \quad (44)$$

The coefficient of $|\psi_T^{(\Lambda)}(r=0)|^2$ is larger than the coefficient of $|\psi_T(r=0)|^2$ in Eq. (42) by the factor $2/(1+Z_{0+})$, which is 1.45 if $\Lambda=m_\pi$.

VII. PRODUCTION OF T_{cc}^+ AND A SOFT PION

In this section, we consider the production of T_{cc}^+ and a soft pion. Our treatment of the triangle-singularity peaks is similar to that for the prompt production of X and a soft pion in Ref. [46]. We also consider the production of T_{cc}^+ and a pion with larger relative momentum.

A. Triangle-Singularity Peaks

1. Amplitude for $T_{cc}^+\pi^+$

Charm mesons $D^{*+}D^{*+}$ created at short distances can rescatter into $T_{cc}^+\pi^+$. The Feynman diagram in XEFT for the production of $T_{cc}^+\pi^+$ from the creation of $D^{*+}D^{*+}$ at a point is shown in Fig. 6. The blob on the left side is the vertex factor $i\mathcal{A}^{ij}_{D^{*+}D^{*+}+y}$ for creating $D^{*+}D^{*+}$ at a point while producing additional particles y with large momenta in the $D^{*+}D^{*+}$ CM frame. The vertex factor is symmetric in the vector indices ij. The D^{*+}-to-$D^0\pi^+$ vertex is given in Eq. (18). The $D^{*+}D^0$-to-T_{cc}^+ vertex is given in Eq. (17).

We take the relative momentum of $T_{cc}^+\pi^+$ in their CM frame to be $\boldsymbol{q}$. The integral over the loop energy in the diagram in Fig. 6 is conveniently evaluated by contours using the pole of the propagator for the D^{*+} line attached to the T_{cc}^+. The resulting amplitude for producing $T_{cc}^+\pi^+$ is

$$\mathcal{A}_{T_{cc}^+\pi^++y}(\boldsymbol{q})=i\left(\mathcal{A}^{ij}_{D^{*+}D^{*+}+y}\sqrt{M_Tm/M_*^2}\right)4\pi G_\pi M_*\sqrt{\gamma_T}\varepsilon^{i*}\int\frac{d^3k}{(2\pi)^3}\frac{1}{(\boldsymbol{k}+(\mu/M)\boldsymbol{q})^2+\gamma^2}\frac{q^j+(m/M_*)k^j}{\boldsymbol{k}^2-(\mu/\mu_\pi)\boldsymbol{q}^2+M_*E_+}, \quad (45)$$

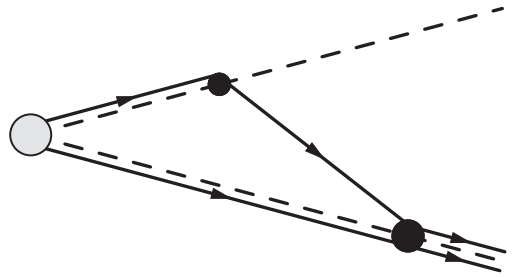

FIG. 6. Feynman diagram in XEFT for D^*D^* created at a point to rescatter into $T_{cc}^+\pi$. The pion is represented by a dashed line.

where $\boldsymbol{\varepsilon}$ is the polarization vector for T_{cc}^+ and $G_\pi = \sqrt{g^2/4\pi m f_\pi^2}$. The factor $\sqrt{M_T m/M_*^2}$ takes into account the difference between relativistic and nonrelativistic normalizations of states. The integral is over the loop momentum $\boldsymbol{k}$ of the D^{*+} that becomes a constituent of T_{cc}^+. In the first denominator in the integrand, γ is the complex binding momentum, $\gamma^2 = -2\mu(\varepsilon_T + i\Gamma_{*+}/2)$, where $\Gamma_{*+} = 83$ keV is the D^{*+} decay width. In the second denominator, E_+ is the complex energy

$$E_+ = \delta_{0+} - \varepsilon_T - i\Gamma_{*+}, \tag{46}$$

where $\delta_{0+} = M_{*+} - M_0 - m_+ = 5.9$ MeV. A necessary (but not necessarily sufficient) condition for the validity of the amplitude in Eq. (45) is that the integral should be dominated by regions in which the relative momentum between the two charm mesons connected to T_{cc}^+ is less than order m_π. If we require the relative momentum to be less than $m_\pi/2$, m_π, or $2m_\pi$, the total kinetic energy $E = q^2/(2\mu_{\pi T})$ of $T_{cc}^+\pi^+$ is required to be less than 7, 12, or 32 MeV.

The two denominators in Eq. (45) can be combined into a single denominator by introducing an integral over a Feynman parameter. After evaluating the integral over the loop momentum, the amplitude for producing $T_{cc}^+\pi^+$ can be reduced to the form

$$\mathcal{A}_{T_{cc}^+\pi^+ +y}(\boldsymbol{q}) = -G_\pi\sqrt{M_T m\gamma_T/4}\,\mathcal{A}^{ij}_{D^{*+}D^{*+}+y}\varepsilon^{i*}q^j T_+(q^2,\gamma^2). \tag{47}$$

The triangle amplitude $T_+(q^2,\gamma^2)$ depends on its two explicit arguments and also on the complex energy E_+ in Eq. (46). It can be expressed as a Feynman parameter integral of the form

$$T_+(q^2,\gamma^2) = \int_0^1 dx \frac{1-(m/M_T)x}{\sqrt{a+bx+cx^2}}. \tag{48}$$

The integral over x in Eq. (48) can be evaluated analytically,

$$T_+(q^2,\gamma^2) = \left(1+\frac{mb}{2M_T c}\right)\frac{1}{\sqrt{c}}\log\frac{\sqrt{a}+\sqrt{c}+\sqrt{a+b+c}}{\sqrt{a}-\sqrt{c}+\sqrt{a+b+c}} + \frac{m}{M_T c}(\sqrt{a}-\sqrt{a+b+c}). \tag{49}$$

The coefficients in these equations are

$$a = (\mu/\mu_\pi)q^2 - M_* E_+, \tag{50a}$$

$$b = -2(\mu/\mu_\pi)(\mu/M)q^2 + M_* E_+ - \gamma^2, \tag{50b}$$

$$c = (\mu/M)^2 q^2. \tag{50c}$$

Note that $a+b+c$ does not depend on q^2, and it approaches 0 in the limits $\varepsilon_T \to 0$, $\Gamma_{*+} \to 0$. Its square root is $\sqrt{a+b+c} = i\gamma$.

The denominator of the argument of the logarithm in Eq. (49) has a zero at a complex value of q^2 that approaches the real axis in the limit where the binding energy $|\varepsilon_T|$ and the width Γ_{*+} both go to zero. This is the triangle singularity. It is convenient to express the singularity in terms of the total kinetic energy $E = q^2/(2\mu_{\pi T})$ of $T_{cc}^+\pi^+$. The triangle amplitude $T_+(q^2,\gamma^2)$ has a logarithmic branch point at the triangle-singularity energy

$$E_{\Delta+} = \frac{M_*}{4\mu^2}\left(\sqrt{2\mu E_+ - \gamma^2} - i\sqrt{m/M_T}\gamma\right)^2. \tag{51}$$

This is the complex energy where the three charm-meson lines that form a triangle in the Feynman diagram in Fig. 6 are all simultaneously on shell. The limit of the triangle-singularity energy as $\varepsilon_T \to 0$, $\Gamma_{*+} \to 0$ is

$$E_{\Delta+} \to (M_T/2M)\delta_{0+} = 6.1 \text{ MeV}. \tag{52}$$

The triangle amplitude $T_+(q^2,\gamma^2)$ also has a square-root branch point at $E = E_+$ from the $\sqrt{a}$ terms in Eq. (49). The limiting behavior of $T_+(q^2,\gamma^2)$ near the triangle singularity is determined by the interplay between the singularities at $E_{\Delta+}$ and E_+, as discussed in Appendix A.

2. Amplitude for $T_{cc}^+\pi^0$

Charm mesons $D^{*+}D^{*0}$ created at short distances can rescatter into $T_{cc}^+\pi^0$. In the Feynman diagram in Fig. 6, the vertex factor for the creation of $D^{*+}D^{*0}$ at a point is $i\mathcal{A}^{ij}_{D^{*+}D^{*0}+y}$. The amplitude for producing $T_{cc}^+\pi^0$ with small relative momentum $\boldsymbol{q}$ in their CM frame is

$$\mathcal{A}_{T_{cc}^+\pi^0+y}(\boldsymbol{q}) = -G_\pi\sqrt{M_T m\gamma_T/8}\,\mathcal{A}^{ij}_{D^{*+}D^{*0}+y}\varepsilon^{i*}q^j T_0(q^2,\gamma^2). \tag{53}$$

The triangle amplitude $T_0(q^2,\gamma^2)$ is given by the right side of Eq. (49) with E_+ in the coefficients a and b replaced by the complex energy

$$E_0 = \delta_{00} - \varepsilon_T - i(\Gamma_{*0} + \Gamma_{*+})/2, \tag{54}$$

where $\delta_{00} = M_{*0} - M_0 - m_0 = 7.0$ MeV and $\Gamma_{*0} \approx 55$ keV is the predicted decay width of D^{*0}.

The amplitude $T_0(q^2, \gamma^2)$ has a triangle singularity from the logarithm in Eq. (49). The logarithmic branch point is at the complex triangle-singularity energy

$$E_{\Delta 0} = \frac{M_*}{4\mu^2}\left(\sqrt{2\mu E_0 - \gamma^2} - i\sqrt{m/M_T}\gamma\right)^2. \tag{55}$$

The limit of the triangle-singularity energy as $\varepsilon_T \to 0$, $\Gamma_{*+} \to 0$, $\Gamma_{*0} \to 0$ is

$$E_{\Delta 0} \to (M_T/2M)\delta_{00} = 7.3 \text{ MeV}. \tag{56}$$

The triangle amplitude $T_0(q^2, \gamma^2)$ also has a square-root branch point at $E = E_0$.

3. Cross sections

The inclusive differential cross section for producing $T_{cc}^+\pi^+$ with small relative momentum $\boldsymbol{q}$ in their CM frame can be expressed as

$$d\sigma[T_{cc}^+\pi^+] = \frac{1}{\text{flux}} \sum_{T_{cc}^+ \text{ spins}} \sum_y \int d\Phi_{(D^*D^*)+y} |\mathcal{A}_{T_{cc}^+\pi^+ + y}(\boldsymbol{q})|^2 \times \frac{d^3q}{(2\pi)^3 2\mu_{\pi T}}, \tag{57}$$

where $d\Phi_{(D^*D^*)+y}$ is defined after Eq. (22). The relativistic differential phase space for $T_{cc}^+\pi^+$ has been expressed as the product of the differential phase space $d^3P/[(2\pi)^3 2P_0]$ for the composite particle (D^*D^*) and $d^3q/[(2\pi)^3 2\mu_{\pi T}]$, where $\mu_{\pi T}$ is the $T_{cc}^+\pi^+$ reduced mass. The differential cross section for producing $T_{cc}^+\pi^0$ is obtained by replacing $\mathcal{A}_{T_{cc}^+\pi^+ + y}(\boldsymbol{q})$ in Eq. (57) by $\mathcal{A}_{T_{cc}^+\pi^0 + y}(\boldsymbol{q})$. The weighted average $\langle \mathcal{A}^{ij}_{D^*D^*}(\mathcal{A}^{kl}_{D^*D^*})^*\rangle$ of the product of short-distance amplitudes is defined by Eq. (22) followed by the average over the spin states of the colliding protons and over the directions of their momenta in the $T_{cc}^+\pi$ rest frame. After multiplying by $(\varepsilon^i q^j)^*(\varepsilon^k q^l)$, the weighted averages can be simplified using Eqs. (25) and (30). The sum over the spin states of T_{cc}^+ results in a factor q^2,

$$\sum_{T_{cc}^+ \text{ spins}} \langle \mathcal{A}^{ij}_{D^{*+}D^{*+}}(\mathcal{A}^{kl}_{D^{*+}D^{*+}})^*\rangle (\varepsilon^i q^j)^*(\varepsilon^k q^l) = 2q^2 \langle \mathcal{A}_{D^+D^+}(\mathcal{A}_{D^+D^+})^*\rangle, \tag{58a}$$

$$\sum_{T_{cc}^+ \text{ spins}} \langle \mathcal{A}^{ij}_{D^{*+}D^{*0}}(\mathcal{A}^{kl}_{D^{*+}D^{*0}})^*\rangle (\varepsilon^i q^j)^*(\varepsilon^k q^l) = 3q^2 \langle \mathcal{A}_{D^+D^0}(\mathcal{A}_{D^+D^0})^*\rangle. \tag{58b}$$

The total kinetic energy $E = q^2/(2\mu_{\pi T})$ of $T_{cc}^+\pi$ in their CM frame is called the invariant kinetic energy, because it is invariant under Galilean boosts. The differential cross sections for $T_{cc}^+\pi^+$ and $T_{cc}^+\pi^0$ as functions of E are

$$\frac{d\sigma}{dE}[T_{cc}^+\pi^+] = \langle \mathcal{A}_{D^+D^0}(\mathcal{A}_{D^+D^0})^*\rangle \frac{G_\pi^2 M_T m \gamma_T}{4\pi^2} \times (2\mu_{\pi T}E)^{3/2} |T_+(2\mu_{\pi T}E, \gamma^2)|^2, \tag{59a}$$

$$\frac{d\sigma}{dE}[T_{cc}^+\pi^0] = \langle \mathcal{A}_{D^+D^0}(\mathcal{A}_{D^+D^0})^*\rangle \frac{3G_\pi^2 M_T m \gamma_T}{32\pi^2} \times (2\mu_{\pi T}E)^{3/2} |T_0(2\mu_{\pi T}E, \gamma^2)|^2, \tag{59b}$$

where $G_\pi^2 = g^2/(4\pi m f_\pi^2)$. We have used Eq. (33) to express both cross sections in terms of the same short-distance factor $\langle \mathcal{A}_{D^+D^0}(\mathcal{A}_{D^+D^0})^*\rangle$ that appears in the cross section for T_{cc}^+ in Eq. (42). These cross sections depend on ε_T through the explicit factor of γ_T and through the triangle amplitudes T_+ and T_0.

The dependence of the differential cross sections $d\sigma/dE$ for $T_{cc}^+\pi^+$ and $T_{cc}^+\pi^0$ on the invariant kinetic energy E is illustrated in Fig. 7 for three values of the T_{cc}^+ binding energy: $|\varepsilon_T| = 320$, 360, and 400 keV. The differential cross sections for $T_{cc}^+\pi^+$ and $T_{cc}^+\pi^0$ each has a narrow peak near the limiting triangle-singularity energy $E_{\Delta+}$ in Eq. (52) and $E_{\Delta 0}$ in Eq. (56), respectively. The full width at half maximum of the peak is about 1 MeV. As $|\varepsilon_T|$ decreases, the energy at the peak approaches the limiting triangle-singularity energy. It decreases through that energy when $|\varepsilon_T|$ decreases below about 0.1 MeV. The shape of $d\sigma/dE$ near the peak is determined by the interplay between the logarithmic

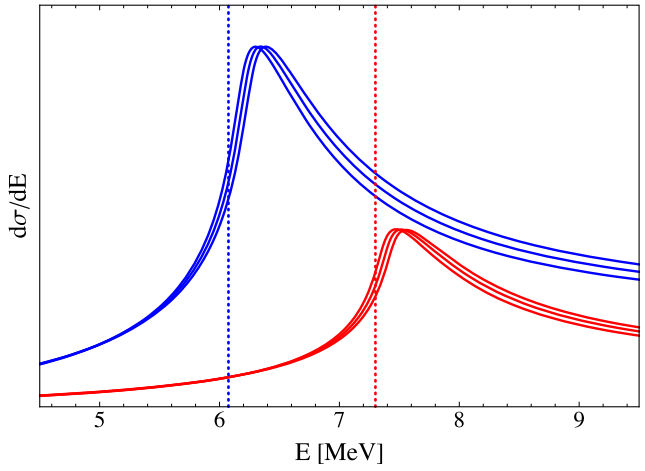

FIG. 7. Differential cross sections $d\sigma/dE$ from Eqs. (59) as functions of the invariant kinetic energy E for $T_{cc}^+\pi^+$ (left blue curves) and for $T_{cc}^+\pi^0$ (right red curves). The binding energies of T_{cc}^+ are 320 keV, 360 keV, and 400 keV in order of increasing energy at the peak. The vertical dotted lines are at the limiting triangle-singularity energies in Eqs. (52) and (56). The scale on the vertical axis is arbitrary.

singularity and the square-root singularity in the triangle amplitude. Beyond the triangle-singularity peaks, the cross sections predicted by Eqs. (59) decrease to a local minimum and then begin to increase. The energy at the local minimum is insensitive to ε_T: $E_{\min,+} = 17.5$ MeV for $T_{cc}^+\pi^+$ and $E_{\min,0} = 21.2$ MeV for $T_{cc}^+\pi^0$.

We would like quantitative estimates of the contributions to the cross sections for $T_{cc}^+\pi^+$ and $T_{cc}^+\pi^0$ from the triangle-singularity peaks. To quantify such a cross section, it is necessary to make a model for the background under the peak. A simple model for the background for $d\sigma/dE$ can be obtained by interpolating between the leading power of E at small E, which is $E^{3/2}$, and a constant at large E equal to the value of $d\sigma/dE$ at the local minimum. The factor $q^3|T_+(q^2,\gamma^2)|^2$ in the differential cross section $d\sigma/dE$ for the production of $T_{cc}^+\pi^+$ has a local minimum at a momentum $q_{\min,+} = \sqrt{2\mu_{\pi T}E_{\min,+}}$ well above the triangle-singularity peak. Our model for the background function for $T_{cc}^+\pi^+$ is

$$q^3|T_+^{(\mathrm{bg})}(q^2,\gamma^2)|^2 = n((E-M_T\delta_{0+}/2M)/\Gamma_\times)q^3|T_+(0,\gamma^2)|^2 + [1-n((E-M_T\delta_{0+}/2M)/\Gamma_\times)]q_{\min,+}^3|T_+(q_{\min,+}^2,\gamma^2)|^2, \quad (60)$$

where $n(x) = 1/(e^x+1)$ and $E = q^2/(2\mu_{\pi T})$. Our model for the background function for $T_{cc}^+\pi^0$ can be obtained from Eq. (60) by replacing $T_+(q^2,\gamma^2)$ by $T_0(q^2,\gamma^2)$, δ_{0+} by δ_{00}, and $q_{\min,+}$ by $q_{\min,0}$. The adjustable parameter $\Gamma_\times$ in Eq. (60) controls the width of the crossover from $q^3|T_+(0,\gamma^2)|^2$ to the constant $q_{\min,+}^3|T_+(q_{\min,+}^2,\gamma^2)|^2$. We choose $\Gamma_\times = 1$ MeV. The resulting background curves for $T_{cc}^+\pi^+$ and $T_{cc}^+\pi^0$ are shown in Fig. 8.

We denote the peaks in the cross sections above the background curves by $(T_{cc}^+\pi^+)_\Delta$ and $(T_{cc}^+\pi^0)_\Delta$. The cross sections for $(T_{cc}^+\pi^+)_\Delta$ and $(T_{cc}^+\pi^0)_\Delta$ can be estimated by integrating over the regions below the curves given by Eqs. (59) and above the corresponding backgrounds from the threshold to the local minimum. The integrated cross sections for producing $(T_{cc}^+\pi)_\Delta$ can be expressed in terms of the cross section for producing T_{cc}^+ without an accompanying soft pion by eliminating the short-distance factor using Eq. (42),

$$\sigma[(T_{cc}^+\pi^+)_\Delta] \approx (8.6\pm0.5)\times10^{-3}\frac{m_\pi^2\gamma_T/2\pi}{|\psi_T(r=0)|^2}\sigma[T_{cc}^+,\mathrm{no}\,\pi], \quad (61a)$$

$$\sigma[(T_{cc}^+\pi^0)_\Delta] \approx (4.8\pm0.2)\times10^{-3}\frac{m_\pi^2\gamma_T/2\pi}{|\psi_T(r=0)|^2}\sigma[T_{cc}^+,\mathrm{no}\,\pi]. \quad (61b)$$

The errors in the numerical prefactors come from the uncertainty in the binding energy $|\varepsilon_T| = 360\pm40$ keV. The largest uncertainty comes from the factor $(m_\pi^2\gamma_T/2\pi)/|\psi_T(r=0)|^2$. Using the expression for the universal wave function at the origin in Eq. (4), this factor can be approximated by $(m_\pi/\Lambda)^2$, where Λ is the ultraviolet cutoff. If Λ is larger or smaller than m_π by a factor of 2, that factor is smaller or larger than 1 by a factor of 4.

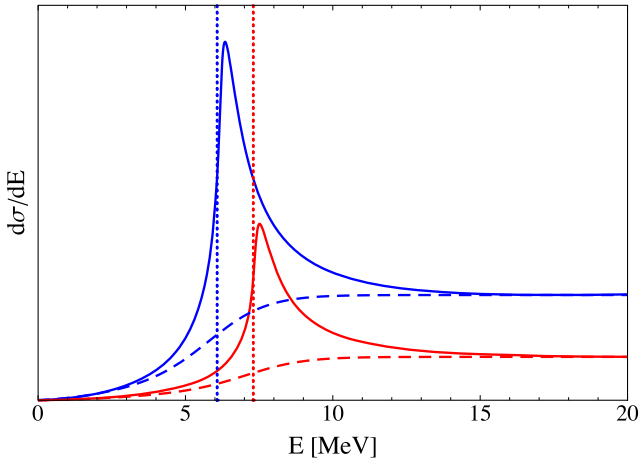

FIG. 8. Differential cross sections $d\sigma/dE$ from Eqs. (59) as functions of the invariant kinetic energy E for $T_{cc}^+\pi^+$ (left blue curves) and for $T_{cc}^+\pi^0$ (right red curves). The binding energy of T_{cc}^+ is $|\varepsilon_T| = 360$ keV. The dashed curves are simple models for the backgrounds. The vertical dotted lines are at the limiting triangle-singularity energies in Eqs. (52) and (56). The scale on the vertical axis is arbitrary.

B. Coupled-channel model

1. Cross sections

The limiting behavior of the triangle amplitude $T_+(q^2,\gamma^2)$ at large q^2 is determined in Eq. (A3) of Appendix A: $T_+(q^2,\gamma^2) \to 0.724/q$. The triangle amplitude $T_0(q^2,\gamma^2)$ has the same limiting behavior. The differential cross sections $d\sigma/dE$ for $T_{cc}^+\pi^+$ and $T_{cc}^+\pi^0$ in Eqs. (59) therefore increase asymptotically as $E^{1/2}$ at large E. This unphysical behavior is an artifact of using the universal approximation for T_{cc}^+ beyond its range of applicability.

The coupled-channel model introduced in Sec. II is a simple model with universal behavior at long distances and more physical qualitative behavior at short distances. The model is specified by wave functions for both the $D^{*+}D^0$

and $D^{*0}D^+$ components of T_{cc}^+, whose parameters are the binding momenta γ_T and γ_{0+} and a larger momentum scale Λ that we assume to be order m_π. The model can be implemented by making the substitutions in Eqs. (19) and (20) in amplitudes from XEFT. The model gives predictions for the production of not only $T_{cc}^+\pi^+$ and $T_{cc}^+\pi^0$ but $T_{cc}^+\pi^-$ as well. The amplitudes in the coupled-channel model are given in Appendix B. They are expressed in terms of simple triangle amplitudes T_+, T_0, and T_- that do not depend on Λ. The amplitude for $T_{cc}^+\pi^+$ has a contribution only from the $D^{*+}D^0$ component of T_{cc}^+. The amplitude for $T_{cc}^+\pi^-$ has a contribution only from the $D^{*0}D^+$ component of T_{cc}^+. The amplitude for $T_{cc}^+\pi^0$ has contributions from both the $D^{*+}D^0$ and $D^{*0}D^+$ components of T_{cc}^+ with short-distance factors $\mathcal{A}^{ij}_{D^{*+}D^{*0}+y}$ and $\mathcal{A}^{ij}_{D^{*0}D^{*+}+y}$, respectively. The cross section for $T_{cc}^+\pi^0$ has interference terms with the short-distance factors $\langle \mathcal{A}^{ij}_{D^{*0}D^{*+}}(\mathcal{A}^{kl}_{D^{*+}D^{*0}})^*\rangle$ and $\langle \mathcal{A}^{ij}_{D^{*+}D^{*0}}(\mathcal{A}^{kl}_{D^{*0}D^{*+}})^*\rangle$. They are suppressed by the random phases in the sum over the many additional particles y. The terms with the short-distance factors $\langle \mathcal{A}^{ij}_{D^{*+}D^{*0}}(\mathcal{A}^{kl}_{D^{*+}D^{*0}})^*\rangle$ and $\langle \mathcal{A}^{ij}_{D^{*0}D^{*+}}(\mathcal{A}^{kl}_{D^{*0}D^{*+}})^*\rangle$ are not suppressed, because they are sums of positive quantities. The short-distance factors in the cross sections for $T_{cc}^+\pi^+$, $T_{cc}^+\pi^0$, and $T_{cc}^+\pi^-$ can be reduced to the same factor $\langle \mathcal{A}_{D^+D^0}(\mathcal{A}_{D^+D^0})^*\rangle$ as in the cross section for T_{cc}^+ in Eq. (44).

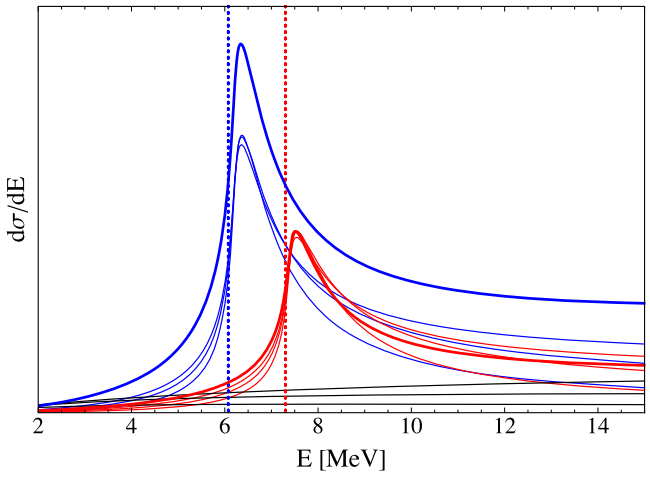

FIG. 9. Differential cross sections $d\sigma/dE$ as functions of the invariant kinetic energy E for $T_{cc}^+\pi^+$ (left blue curves), $T_{cc}^+\pi^0$ (right red curves), and $T_{cc}^+\pi^-$ (lower black curves). The binding energy of T_{cc}^+ is $|\varepsilon_T| = 360$ keV. The thicker curves for $T_{cc}^+\pi^+$ and $T_{cc}^+\pi^0$ were calculated using Eqs. (59). The thinner curves for the coupled-channel model were calculated using Eqs. (62), with $\Lambda/m_\pi = 1/2$, 1, and 2 in order of increasing cross sections at small E and at large E. The vertical dotted lines are at the limiting triangle-singularity energies in Eqs. (52) and (56). The scale on the vertical axis is arbitrary.

The differential cross sections for $T_{cc}^+\pi^+$, $T_{cc}^+\pi^0$, and $T_{cc}^+\pi^-$ in the coupled-channel model as functions of the invariant kinetic energy E are

$$\frac{d\sigma}{dE}[T_{cc}^+\pi^+] = \langle \mathcal{A}_{D^+D^0}(\mathcal{A}_{D^+D^0})^*\rangle \frac{G_\pi^2 M_T m \gamma_T}{4\pi^2}(2\mu_{\pi T}E)^{3/2}|T_+^{(\Lambda)}(2\mu_{\pi T}E,\gamma^2)|^2, \tag{62a}$$

$$\frac{d\sigma}{dE}[T_{cc}^+\pi^0] = \langle \mathcal{A}_{D^+D^0}(\mathcal{A}_{D^+D^0})^*\rangle \frac{3G_\pi^2 M_T m \gamma_T}{32\pi^2}(2\mu_{\pi T}E)^{3/2}(|T_0^{(\Lambda)}(2\mu_{\pi T}E,\gamma^2)|^2 + |T_0'^{(\Lambda)}(2\mu_{\pi T}E,\gamma_{0+}^2)|^2), \tag{62b}$$

$$\frac{d\sigma}{dE}[T_{cc}^+\pi^-] = \langle \mathcal{A}_{D^+D^0}(\mathcal{A}_{D^+D^0})^*\rangle \frac{G_\pi^2 M_T m \gamma_T}{4\pi^2}(2\mu_{\pi T}E)^{3/2}|T_-^{(\Lambda)}(2\mu_{\pi T}E,\gamma_{0+}^2)|^2. \tag{62c}$$

The triangle amplitudes $T_+^{(\Lambda)}$, $T_0^{(\Lambda)}$, $T_0'^{(\Lambda)}$, and $T_-^{(\Lambda)}$ are given in Appendix B in Eqs. (B1), (B7), (B9), and (B6). The differential cross sections $d\sigma/dE$ are shown in Fig. 9 for $|\varepsilon_T| = 360$ keV and three values of the momentum scale Λ: $\Lambda/m_\pi = 1/2$, 1, and 2. The cross sections for $T_{cc}^+\pi^+$ and $T_{cc}^+\pi^0$ with the universal triangle amplitudes are also shown. The triangle-singularity peaks for $T_{cc}^+\pi^+$ and $T_{cc}^+\pi^0$ in the coupled-channel model have essentially the same shape as those with the universal triangle amplitudes. The height of the peak for $T_{cc}^+\pi^+$ in the coupled-channel model is smaller by the multiplicative factor $1/(1+Z_{0+})$, which is 0.73 for $\Lambda = m_\pi$. The height of the peak for $T_{cc}^+\pi^0$ in the coupled-channel model is approximately equal to that with the universal triangle amplitude. This is the result of a fortuitous compensation between the multiplicative factor $1/(1+Z_{0+})$ and the additional contribution from the $D^{*0}D^+$ component of T_{cc}^+. The limiting behaviors of $T_0(q^2,\gamma^2)$ and $T_0(q^2,\gamma_{0+}^2)$ near the triangle singularity can be deduced from the limiting behavior of $T_+(q^2,\gamma^2)$ determined in Eq. (A2) of Appendix A. The ratio of the contributions to the cross section at the triangle-singularity peak from the $D^{*0}D^+$ and $D^{*+}D^0$ components of T_{cc}^+ can be approximated by the absolute square of the ratio of the logarithms in $T_0^{(\log)}(q^2,\gamma_{0+}^2)$ and $T_0^{(\log)}(q^2,\gamma^2)$ at $q^2 = q_{\Delta 0}^2$, which is equal to 0.36 for $|\varepsilon_T| = 360$ keV. This ratio is close to the value $Z_{0+} = 0.38$ for $\Lambda = m_\pi$. There is no triangle singularity in the production of $T_{cc}^+\pi^-$, because the mass of D^{*0} is 2.4 MeV below the threshold for decay into

$D^+\pi^-$. This prevents the D^{*0} and D^+ lines in the triangle diagram from being simultaneously on shell. The cross sections for $T_{cc}^+\pi^-$ are therefore small and slowly increasing in the region where the cross sections for $T_{cc}^+\pi^+$ and $T_{cc}^+\pi^0$ have narrow peaks. At energies above the peaks, there is a significant decrease in all three cross sections as Λ decreases. The dependence on Λ demonstrates that the cross sections above the triangle-singularity peaks are model dependent.

2. High-energy limits

The asymptotic behavior at large q^2 of the triangle amplitude $T_+^{(\Lambda)}(q^2,\gamma^2)$ is determined in Eq. (B11) of Appendix B. It decreases asymptotically as $1/q^2$, with a coefficient that has a factor of $\psi_T^{(\Lambda)}(r=0)$. The other triangle amplitudes $T_0^{(\Lambda)}$, $T_0'^{(\Lambda)}$, and $T_-^{(\Lambda)}$ have the same asymptotic behavior up to a sign. The differential cross sections for $T_{cc}^+\pi^+$, $T_{cc}^+\pi^0$, and $T_{cc}^+\pi^-$ in Eqs. (62) therefore all decrease asymptotically as $E^{-1/2}$ at large E. The multiplicative short-distance factors in the cross sections for $T_{cc}^+\pi$ in Eqs. (62) can be eliminated in favor of the cross section for T_{cc}^+ in Eq. (44). This also eliminates the factors of $|\psi_T^{(\Lambda)}(r=0)|^2$. The resulting expressions for the asymptotic behaviors of the differential cross sections for $T_{cc}^+\pi^+$, $T_{cc}^+\pi^0$, and $T_{cc}^+\pi^-$ are

$$\frac{d\sigma}{dE}[T_{cc}^+\pi^+] \to \sigma^{(\Lambda)}[T_{cc}^+,\mathrm{no}\,\pi]\frac{8G_\pi^2\mu_{\pi T}^2\mu_\pi}{3\pi}(2\mu_{\pi T}E)^{-1/2}, \quad (63a)$$

$$\frac{d\sigma}{dE}[T_{cc}^+\pi^0] \to \sigma^{(\Lambda)}[T_{cc}^+,\mathrm{no}\,\pi]\frac{2G_\pi^2\mu_{\pi T}^2\mu_\pi}{\pi}(2\mu_{\pi T}E)^{-1/2}, \quad (63b)$$

$$\frac{d\sigma}{dE}[T_{cc}^+\pi^-] \to \sigma^{(\Lambda)}[T_{cc}^+,\mathrm{no}\,\pi]\frac{8G_\pi^2\mu_{\pi T}^2\mu_\pi}{3\pi}(2\mu_{\pi T}E)^{-1/2}. \quad (63c)$$

In Fig. 10, the differential cross section for $T_{cc}^+\pi^+$ in Eq. (62a) divided by $\sigma^{(\Lambda)}[T_{cc}^+,\mathrm{no}\,\pi]$ is compared with the asymptotic cross section in Eq. (63a) for $\Lambda/m_\pi = 1/2$, 1, and 2. The height of the triangle-singularity peak depends dramatically on Λ, but the curves all approach the asymptotic cross section as E increases.

The cross section $\sigma^{(\Lambda)}[T_{cc}^+,\mathrm{no}\,\pi]$ on the right sides of Eqs. (63) should not be interpreted literally as the cross section for T_{cc}^+ without any pion. It is actually the cross section for T_{cc}^+ without any pion with relative momentum smaller than the ultraviolet cutoff $q_{\max}$ used to define the short-distance amplitudes. The momentum $q_{\max}$ is an arbitrary scale separating states described explicitly by the effective field theory from states described implicitly through the dependence of short-distance amplitudes on $q_{\max}$. A pion with relative momentum less than $q_{\max}$ is described explicitly. The effects of pions with relative momentum larger than $q_{\max}$ must be taken into account through the short-distance amplitudes. In the case of $T_{cc}^+\pi$ states, the corresponding invariant kinetic energy is $E_{\max} = q_{\max}^2/(2\mu_{\pi T})$. As $E_{\max}$ is increased, there are T_{cc}^+ events with no pion that are resolved into $T_{cc}^+\pi^+$, $T_{cc}^+\pi^0$, and $T_{cc}^+\pi^-$ events, so $\sigma^{(\Lambda)}[T_{cc}^+,\mathrm{no}\,\pi]$ must decrease accordingly. The sum of $\sigma^{(\Lambda)}[T_{cc}^+,\mathrm{no}\,\pi]$ and the cross sections for $T_{cc}^+\pi^+$, $T_{cc}^+\pi^0$, and $T_{cc}^+\pi^-$ integrated over $E < E_{\max}$ should not depend on $E_{\max}$. This condition requires short-distance factors of the form $\langle \mathcal{A}_{D^*D}(\mathcal{A}_{D^*D})^*\rangle$ to be multiplied by a factor whose difference from 1 is order $G_\pi^2\mu_{\pi T}\mu_\pi q_{\max}$. Since $G_\pi^2\mu_{\pi T}\mu_\pi m_\pi = 0.027$, the multiplicative factor is close to 1 if $q_{\max} < m_\pi$. We have therefore not implemented the multiplicative factors that guarantee that cross sections are independent of $q_{\max}$.

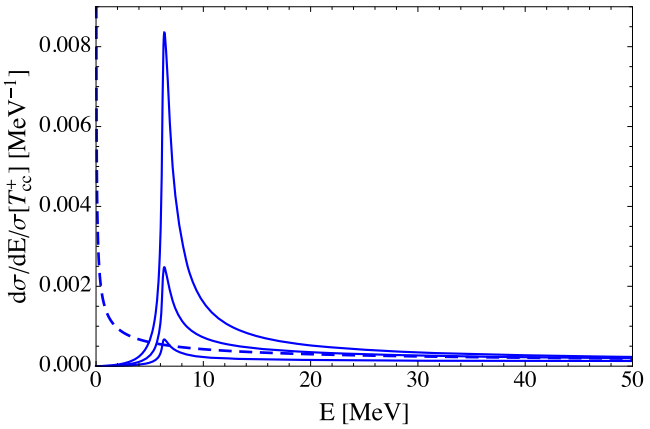

FIG. 10. Differential cross sections $d\sigma/dE$ divided by $\sigma^{(\Lambda)}[T_{cc}^+,\mathrm{no}\,\pi]$ as functions of the invariant kinetic energy E for $T_{cc}^+\pi^+$. The binding energy of T_{cc}^+ is $|\varepsilon_T| = 360$ keV. The solid curves are calculated using the triangle amplitude $T_+^{(\Lambda)}$ with $\Lambda/m_\pi = 1/2$, 1, and 2 in order of decreasing cross sections. The dashed curve is the asymptotic result from Eq. (63a). The scale on the vertical axis is in units of 1/MeV.

We would like quantitative estimates of the integrated cross sections for T_{cc}^+ accompanied by a soft pion. The differential cross sections for $T_{cc}^+\pi^+$, $T_{cc}^+\pi^0$, and $T_{cc}^+\pi^-$ in the coupled-channel model are given in Eqs. (62). Their high-energy limits in Eqs. (63) show that the cross sections integrated over the energy E up to some maximum $E_{\max}$ increase asymptotically as $E_{\max}^{1/2}$. As shown in Appendix B 4, this is the correct asymptotic behavior for a general wave function. The cross sections integrated up to an energy $E_{\max}$ much larger than the limiting triangle-singularity energies can be expressed as

$$\sigma[T_{cc}^+\pi^+] \approx \left(3.2\sqrt{\frac{E_{\max}}{m_\pi}} - 0.0^{+1.8}_{-1.3}\right)\times 10^{-2}\sigma^{(\Lambda)}[T_{cc}^+,\mathrm{no}\,\pi], \quad (64a)$$

$$\sigma[T_{cc}^+\pi^0] \approx \left(2.4\sqrt{\frac{E_{\max}}{m_\pi}} - 0.0^{+1.3}_{-1.0}\right) \times 10^{-2}\sigma^{(\Lambda)}[T_{cc}^+, \text{no}\,\pi], \tag{64b}$$

$$\sigma[T_{cc}^+\pi^-] \approx \left(3.2\sqrt{\frac{E_{\max}}{m_\pi}} - 1.3^{+0.3}_{-0.5}\right) \times 10^{-2}\sigma^{(\Lambda)}[T_{cc}^+, \text{no}\,\pi]. \tag{64c}$$

The coefficients of $\sqrt{E_{\max}/m_\pi}$ were determined from the asymptotic behaviors of $d\sigma/dE$ in Eqs. (63). The numerical coefficients with error bars were deduced by fitting the subleading behavior at large $E_{\max}$ with $\Lambda = 2^{0\pm1}m_\pi$.

Near the triangle-singularity peak in $d\sigma/dE$ for $T_{cc}^+\pi^+$, the differential cross section for $T_{cc}^+\pi^-$ is much smaller, as is evident in Fig. 9. In experimental measurements of $d\sigma/dE$ for $T_{cc}^+\pi^+$, subtracting $d\sigma/dE$ for $T_{cc}^+\pi^-$ would also remove the background from random pions from the pp collision that have nothing to do with the creation of charm mesons. The difference between the cross sections in the coupled-channel model in Eqs. (62a) and (62c) is shown as a function of E in Fig. 11. Since the differential cross sections for $T_{cc}^+\pi^+$ and $T_{cc}^+\pi^-$ have the same limiting behavior at large E, the difference between their integrated cross sections is independent of $E_{\max}$,

$$\sigma[T_{cc}^+\pi^+] - \sigma[T_{cc}^+\pi^-] \approx (1.3^{+1.5}_{-0.8}) \times 10^{-2}\sigma^{(\Lambda)}[T_{cc}^+, \text{no}\,\pi]. \tag{65}$$

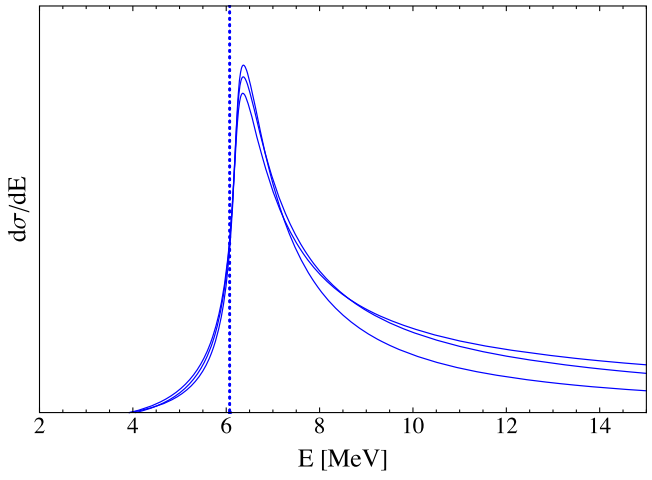

FIG. 11. Difference between the differential cross sections $d\sigma/dE$ for $T_{cc}^+\pi^+$ and $T_{cc}^+\pi^-$ in the coupled-channel model as functions of the invariant kinetic energy E. The binding energy of T_{cc}^+ is $|\varepsilon_T| = 360$ keV. The curves were calculated using Eqs. (62a) and (62c) with $\Lambda/m_\pi = 1/2$, 1, and 2 in order of increasing cross sections at small E and at large E. The vertical dotted line is at the limiting triangle-singularity energy in Eq. (52). The scale on the vertical axis is arbitrary.

This difference is dominated by the triangle-singularity peak. It is roughly compatible with the estimate of the cross section for $(T_{cc}^+\pi^+)_\Delta$ in Eq. (61a), but it has a smaller error bar from varying Λ. We can use the difference in Eq. (65) as an estimate of the contribution to the integrated cross section for $T_{cc}^+\pi^+$ from the triangle-singularity peak.

C. LHCb data

The production of T_{cc}^+ in pp collisions at the LHC has been studied by the LHCb Collaboration [9,10]. The T_{cc}^+ was observed as a peak in the $D^0D^0\pi^+$ invariant mass distribution below the $D^{*+}D^0$ threshold. The number of events in the peak was 117 ± 16. There is also evidence for the decay of T_{cc}^+ into $D^+D^0\pi^0$ in the form of a narrow peak in the invariant mass distribution for D^+D^0 near its threshold.

At a hadron collider, it is much easier to detect a charged pion than a neutral pion. Thus the production rates for T_{cc}^+ accompanied by a π^+ or π^- can be measured. The creation of $D^{*+}D^{*+}$ at short distances can produce T_{cc}^+ accompanied by a soft π^+. The creation of $D^{*0}D^{*0}$ at short distances can produce T_{cc}^+ accompanied by a soft π^-. There may also be $T_{cc}^+\pi^+$ and $T_{cc}^+\pi^-$ events with random pions produced by the pp collision that have nothing to do with the creation of charm mesons at short distances.

The inclusive cross section for T_{cc}^+ is the sum of the cross section $\sigma^{(\Lambda)}[T_{cc}^+, \text{no}\,\pi]$ for T_{cc}^+ without any pion with relative momentum less than $q_{\max}$ and the cross sections $\sigma[T_{cc}^+\pi^+]$, $\sigma[T_{cc}^+\pi^0]$, and $\sigma[T_{cc}^+\pi^-]$ integrated over the invariant kinetic energy up to $E_{\max} = q_{\max}^2/(2\mu_{\pi T})$. The fraction of T_{cc}^+ events accompanied by a soft π^+ or a soft π^- can be estimated using the results in Eqs. (64). The fractions of events having $T_{cc}^+\pi^+$ and $T_{cc}^+\pi^-$ with invariant kinetic energy less than m_π are estimated to be $(3.0^{+1.5}_{-1.2})\%$ and $(1.8^{+0.2}_{-0.4})\%$, respectively. Our estimates suggest that a few of the T_{cc}^+ events observed by the LHCb Collaboration should be accompanied by a soft π^+ with relative momentum less than m_π, and that there should be a smaller but comparable number accompanied by a soft π^-.

The fraction of T_{cc}^+ events with a π^+ in the peak from the triangle singularity can be estimated using the result in Eq. (65). Our estimate $(1.2^{+1.3}_{-0.7})\%$ suggests that a few of the T_{cc}^+ events observed by the LHCb Collaboration could have a π^+ in the peak from the triangle singularity. While the number of these events is small, they all have invariant kinetic energy E of $T_{cc}^+\pi^+$ within 1 MeV of 6.1 MeV. The creation of charm mesons at short distances should produce essentially no $T_{cc}^+\pi^-$ events in that region of E. The production of $T_{cc}^+\pi^-$ can therefore be used to measure the background from $T_{cc}^+\pi^+$ events with a random π^+ from the pp collision.

VIII. SUMMARY

We have studied the inclusive production of T_{cc}^+ at a high-energy hadron collider through the creation of two charm mesons at short distances. The formation of T_{cc}^+ was described by the effective field theory XEFT. The T_{cc}^+ can be produced by the creation of its constituents $D^{*+}D^0$ at short distances followed by the binding of the charm mesons into T_{cc}^+. The T_{cc}^+ can also be produced by the creation of spin-1 charm mesons D^*D^* at short distances followed by the rescattering of the charm mesons into $T_{cc}^+\pi$. The universality of near-threshold S-wave resonances guarantees that there are aspects of the production that are determined by the binding momentum γ_T of T_{cc}^+. There are also aspects that involve larger momenta comparable to the ultraviolet cutoff Λ of XEFT. Those aspects were studied using a coupled-channel model for the $D^{*+}D^0$ and $D^{*0}D^+$ components of T_{cc}^+ with isospin symmetry at short distances. The coupled-channel model can be defined by the prescriptions in Eqs. (19) and (20).

The T_{cc}^+ can be produced without an accompanying soft pion by the creation of $D^{*+}D^0$ at short distances. The cross section $\sigma[T_{cc}^+, \text{no}\,\pi]$ is expressed in Eq. (42) as the product of a short-distance factor and the square $|\psi_T(r=0)|^2$ of the universal wave function at the origin for T_{cc}^+. The factor $|\psi_T(r=0)|^2$ is sensitive to the binding energy of T_{cc}^+ through a multiplicative factor of γ_T. It is more sensitive to the ultraviolet cutoff Λ, scaling approximately as Λ^2. The cross section $\sigma^{(\Lambda)}[T_{cc}^+, \text{no}\,\pi]$ in the coupled-channel model is given in Eq. (44). It differs from the cross section in Eq. (42) by replacing $|\psi_T(r=0)|^2$ by $|\psi_T^{(\Lambda)}(r=0)|^2/(1+Z_{0+})$ and multiplying by 2 to take into account the $D^{*0}D^+$ component of T_{cc}^+. The factor $|\psi_T^{(\Lambda)}(r=0)|^2$ could in principle be determined from other reactions involving T_{cc}^+, such as the differential cross section for producing $T_{cc}^+\pi^+$ with large invariant kinetic energy.

The T_{cc}^+ can be produced with an accompanying soft π^+ or π^0 by the creation of $D^{*+}D^{*+}$ or $D^{*+}D^{*0}$ at short distances, respectively. In Eqs. (59) the differential cross sections for $T_{cc}^+\pi^+$ and $T_{cc}^+\pi^0$ are expressed in a form with the same short-distance factor as in $\sigma[T_{cc}^+, \text{no}\,\pi]$. The differential cross sections $d\sigma/dE$ are shown in Fig. 7 as functions of the invariant kinetic energy E for $T_{cc}^+\pi$. They have a narrow peak from a triangle singularity about 6.1 MeV above the threshold for $T_{cc}^+\pi^+$ and about 7.3 MeV above the threshold for $T_{cc}^+\pi^0$. Since the peak is near the onset of a D^*D^* threshold, the calculation of the cross section integrated over the peak requires the construction of a smooth background, such as that shown in Fig. 8. Our results for the cross sections for $T_{cc}^+\pi^+$ and $T_{cc}^+\pi^0$ integrated over the triangle-singularity peaks are given in Eqs. (61). The factor $|\psi_T(r=0)|^2$ in the denominator gives a very large uncertainty.

We used the coupled-channel model to calculate the cross sections for $T_{cc}^+\pi^+$, $T_{cc}^+\pi^0$, and $T_{cc}^+\pi^-$ at energies near the triangle-singularity peaks and at higher energies. The differential cross sections at E above the triangle-singularity peaks are sensitive to the momentum scale Λ, as illustrated in Fig. 9. For E well above the peak, the dependence of $d\sigma/dE$ on Λ reduces to a multiplicative factor proportional to $|\psi_T^{(\Lambda)}(r=0)|^2$. The short-distance factor and the factor $|\psi_T^{(\Lambda)}(r=0)|^2$ can be eliminated from $d\sigma/dE$ in favor of $\sigma^{(\Lambda)}[T_{cc}^+, \text{no}\,\pi]$. The resulting differential cross sections for $T_{cc}^+\pi^+$, $T_{cc}^+\pi^0$, and $T_{cc}^+\pi^-$ at large E are given in Eqs. (63). Simple approximations for the cross section integrated over E up to E_{max} are given in Eqs. (64). In the case of $T_{cc}^+\pi^+$ and $T_{cc}^+\pi^0$, the subleading term includes a contribution from the triangle-singularity peak.

The production of T_{cc}^+ accompanied by a soft π^+ can be studied at the LHC, because the charged pion provides a clean signature. Our estimate of the fraction of T_{cc}^+ events accompanied by a π^+ with invariant kinetic energy less than m_π is $(3.0^{+1.5}_{-1.2})\%$. The LHCb Collaboration discovered T_{cc}^+ as a peak in the $D^0D^0\pi^+$ invariant mass distribution [9,10]. The number of events in the peak was 117 ± 16. Our estimate suggests that several of those events should be accompanied by an additional π^+ with relative momentum less than m_π. Our estimate for the fraction of T_{cc}^+ events with $T_{cc}^+\pi^+$ in the narrow peak from the triangle singularity near $E = 6.1$ MeV is $(1.2^{+1.3}_{-0.7})\%$. All of these events would be within 1 MeV of the triangle-singularity energy. There may be some $T_{cc}^+\pi^+$ events near that peak with a random pion from the proton-proton collision that is unrelated to the creation of charm mesons. The background from this contribution can be determined experimentally by measuring $T_{cc}^+\pi^-$ events.

Our calculation of the peak in the cross section for $T_{cc}^+\pi^+$ from a charm-meson triangle singularity is based on the assumption that the charm mesons are created at short distances much smaller than the mean radius $\langle r \rangle$ of T_{cc}^+. This assumption is very well justified for the production of T_{cc}^+ from single-parton scattering. It is less well justified for the production of T_{cc}^+ from double-parton scattering, because the charm mesons may be created at distances comparable to the radius of a proton. The triangle-singularity peak could stand out more clearly above the background in the contribution from SPS. The LHCb Collaboration has observed a larger yield of T_{cc}^+ relative to $D^0\bar{D}^0$ at larger values of the number N_{tracks} of tracks in the vertex detector [10]. If the increased yield at larger multiplicity arises from the DPS mechanism, the restriction to $N_{\text{tracks}} < 80$ could produce a sample of T_{cc}^+ events in which a larger fraction comes from the SPS mechanism. Such a restriction could make the triangle-singularity peak stand out more clearly above the background.

We calculated the cross sections for $T_{cc}^+\pi^+$ and $T_{cc}^+\pi^0$ at low energies near the triangle-singularity peaks using

XEFT at LO. The coupled-channel model we used to calculate the cross sections for $T_{cc}^+\pi^+$, $T_{cc}^+\pi^0$, and $T_{cc}^+\pi^-$ at higher energies agrees with XEFT at leading order at low energy, and at high energy it has power-law behavior compatible with XEFT. It smoothly connects the amplitudes in the intermediate energy region, but in this region it is just a model. It would be worthwhile to extend the accuracy of our calculations to XEFT at next-to-leading order. This effective field theory has been applied to decays of the T_{cc}^+ at leading order in Refs. [22,23] and some next-to-leading order corrections were calculated in Ref. [22]. The calculation of the cross section for $T_{cc}^+\pi^+$ near the peak from the triangle singularity in XEFT at next-to-leading order should be straightforward. A systematically improvable calculation of the cross section at higher energies is a more challenging problem.

We have discussed the effect of the triangle singularity on the production of T_{cc}^+ accompanied by a pion. The triangle singularity also affects the production of the constituents $D^{*+}D^0$ accompanied by a pion. This reaction proceeds through the tree diagram in Fig. 13 and also through the loop diagram obtained from the triangle diagram in Fig. 6 by attaching D^{*+} and D^0 lines to the outgoing T_{cc}^+ line. The two diagrams produce an interesting interference effect called the *Schmid cancellation* [72]. A convenient choice of Dalitz-plot variables is the invariant mass s of $D^{*+}D^0$ and the invariant mass t of $D^0\pi^+$. The triangle singularity appears along the line $s = s_\Delta$, where $s_\Delta = (M_{*+} + M_0 + E_\Delta)^2$. In the limit where the charm mesons in the triangle are all on shell, the differential cross section as a function of s and t has a $\log^2|s - s_\Delta|$ divergence along that line for all values of t inside the Dalitz plot. The Schmid cancellation is that the differential cross section integrated over t has only a single-log divergence $\log|s - s_\Delta|$. The cancellation can be most easily observed through a local minimum as a function of t in the differential cross section integrated over the region $s < s_\Delta$ [55].

At energies well above the triangle singularity energy E_Δ, the differential cross section $d\sigma/dE$ for producing $T_{cc}^+\pi^+$ is predicted to decrease as $E^{-1/2}$. This behavior provides a way of discriminating between a loosely bound charm-meson molecule and a compact tetraquark. A compact tetraquark T would have to have a suppressed coupling to $D^{*+}D^0$; otherwise the resonant interactions of $D^{*+}D^0$ would transform T into a large charm-meson molecule. The Goldstone nature of the pion requires the production amplitude of $T\pi$ to be proportional to the relative momentum of the pion. The differential cross section $d\sigma/dE$ should therefore increase like $E^{3/2}$. Measurements of the production rate of $T_{cc}^+\pi^+$ at energies well above E_Δ would therefore provide important clues to the nature of T_{cc}^+.

Loosely bound S-wave charm-meson molecules like X and T_{cc}^+ have universal properties determined by their binding energies. One of these properties is a narrow peak from a charm-meson triangle singularity in the rate for their production accompanied by a pion. Our estimate of the cross section for $T_{cc}^+\pi^+$ from the triangle-singularity peak is large enough to encourage the effort to observe the peak at the LHC. The observation of such a peak would provide strong support for the identification of T_{cc}^+ as a loosely bound charm-meson molecule.

ACKNOWLEDGMENTS

This work was supported in part by the U.S. Department of Energy under Grant No. DE-SC0011726, by the National Natural Science Foundation of China (NSFC) under Grant No. 11905112, by the Natural Science Foundation of Shandong Province of China under Grant No. ZR2019QA012, and by NSFC and the Deutsche Forschungsgemeinschaft (DFG) through the Sino-German Collaborative Research Center TRR110 Symmetries and the Emergence of Structure in QCD (NSFC Grant No. 12070131001, DFG Project-ID No. 196253076—TRR110).

APPENDIX A: LIMITING BEHAVIOR OF TRIANGLE AMPLITUDES

An analytic expression for the triangle amplitude $T_+(q^2,\gamma^2)$ is given in Eq. (49), where a, b, and c are the coefficients in Eqs. (50). In this appendix we give limiting expressions for this triangle amplitude.

The triangle singularity in $T_+(q^2,\gamma^2)$ comes from the logarithm in Eq. (49). In the simultaneous limits $\varepsilon_T \to 0$, $\Gamma_{*+} \to 0$, the triangle singularity is at the real value $q_{\Delta+}^2 = (M_T/2\mu)m\delta_{0+}$. Near the triangle singularity, the square roots $\sqrt{a}$ and $\sqrt{c}$ in the argument of the logarithm are both comparable to $(\mu/M)q_{\Delta+}$. This can be made more obvious by expressing the coefficient a in Eq. (50a) in the form

$$a = (\mu/M)^2 q_{\Delta+}^2 + (\mu/\mu_\pi)(q^2 - q_{\Delta+}^2) + M_*(\varepsilon_T + i\Gamma_{*+}). \tag{A1}$$

The difference $\sqrt{a} - \sqrt{c}$ can be comparable in magnitude to $\sqrt{a+b+c} = i\gamma$, which is approximately $i\sqrt{2\mu|\varepsilon_T|}$. Near the triangle singularity, $T_+(q^2,\gamma^2)$ can be approximated by simplifying the coefficient of the logarithm in Eq. (49) and the additive term by setting $q^2 = q_{\Delta+}^2$ and taking the limits $\varepsilon_T \to 0$, $\Gamma_{*+} \to 0$,

$$T_+^{(\log)}(q^2,\gamma^2) = \sqrt{\frac{M/M_T}{\mu_\pi \delta_{0+}}}\left(\frac{2M}{M_*}\log\frac{\sqrt{a}+(\mu/M)q+i\gamma}{\sqrt{a}-(\mu/M)q+i\gamma} + \frac{m}{M_*}\right). \tag{A2}$$

The triangle amplitude $T_+(q^2,\gamma^2)$ and the logarithmic approximation in Eq. (A2) are compared in Fig. 12 by

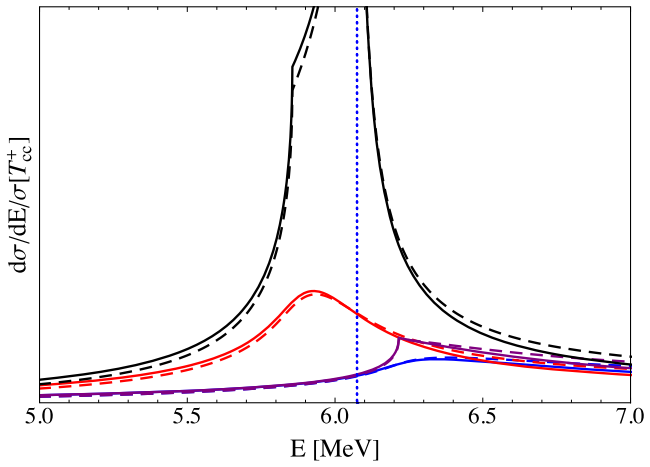

FIG. 12. Differential cross sections $d\sigma/dE$ divided by $\sigma[T_{cc}^+, \text{no}\,\pi]$ as functions of the invariant kinetic energy E for $T_{cc}^+\pi^+$. The cross sections are calculated using the complete triangle amplitude $T_+(q^2,\gamma^2)$ (solid curves) and the logarithmic approximation in Eq. (A2) (dashed curves). The four cases of $(|\varepsilon_T|,\Gamma_{*+})$ in order of increasing height of the peak are (a) (360 keV, 83 keV) (blue curves), (b) (360 keV, 0) (purple curves), (c) (0, 83 keV) (red curves), and (d) (0, 0) (black curves). The scale on the vertical axis is arbitrary.

showing the differential cross section $d\sigma/dE$ for $T_{cc}^+\pi^+$ as a function of the invariant energy E. The differential cross section has been divided by $\sigma[T_{cc}^+, \text{no}\,\pi]$ to ensure that the limit as $\varepsilon_T \to 0$ is nonzero. The logarithmic approximation gives a good fit to the exact curve near the peak not only for $|\varepsilon_T| = 360$ keV, $\Gamma_{*+} = 83$ keV but also in the limit $\varepsilon_T \to 0$, in the limit $\Gamma_{*+} \to 0$, and in the simultaneous limits $\varepsilon_T \to 0$, $\Gamma_{*+} \to 0$. In the limit $\Gamma_{*+} \to 0$, $d\sigma/dE$ develops a cusp at $E = \delta_{0+} - \varepsilon_T$. For $|\varepsilon_T| = 360$ keV, the cusp coincides with the peak, as is evident in Fig. 12. For $\varepsilon_T = 0$, the cusp at $E = \delta_{0+}$ is well separated from the $\log^2$ divergence at $E = M_T/(2M)\delta_{0+}$.

The triangle amplitude $T_+(q^2,\gamma^2)$ has a logarithmic branch point at the complex triangle-singularity energy $E_{\Delta+}$ in Eq. (51) and a square-root branch point at the complex energy E_+ in Eq. (46). These nearby singularities both approach the real axis in the simultaneous limits $\varepsilon_T \to 0, \Gamma_{*+} \to 0$. The leading behavior of $T_+(q^2,\gamma^2)$ near the square-root and logarithmic singularities have the forms $A + B\sqrt{E - E_+}$ and $C + D\log(E - E_{\Delta+})$, respectively, where A, B, C, and D are complex constants that depend on ε_T and Γ_{*+}. In the simultaneous limits $\varepsilon_T \to 0, \Gamma_{*+} \to 0$, the differential cross section $d\sigma/dE$ has a cusp at $E = \delta_{0+}$ and a $\log^2$ divergence at $E = M_T/(2M)\delta_{0+}$ that are both well described by the leading singularities. If $|\varepsilon_T|$ is increased to 360 keV or Γ_{*+} is increased to 83 keV, the peak in $d\sigma/dE$ is not described well by the leading singularities. The leading square-root singularity gives a cross section that is mononotically increasing. The leading logarithmic singularity gives a cross section with a peak whose height is larger by a factor of 3 or more and whose position is at an energy lower by at least 0.3 MeV than that from the complete triangle amplitude. An accurate description of the peak requires the logarithm in Eq. (A2), which involves an interplay between the two singularities.

The triangle amplitude $T_+(q^2,\gamma^2)$ at large q^2 can be expanded in powers of $1/q$. The expansion to next-to-leading order is

$$T_+(q^2,\gamma^2) \to \left(\frac{M}{M_*}\log\frac{\sqrt{M_T/m}+1}{\sqrt{M_T/m}-1} + \frac{\sqrt{M_T m}}{M_*}\right)\frac{1}{q} - \frac{2iM_T m\gamma}{M_*^2 q^2}. \tag{A3}$$

The numerical value of the dimensionless prefactor of $1/q$ is 0.724.

APPENDIX B: TRIANGLE AMPLITUDES IN THE COUPLED-CHANNEL MODEL

In this appendix, we determine the triangle amplitudes in the coupled-channel model using the prescriptions in Eqs. (19) and (20).

1. Amplitude for $T_{cc}^+\pi^+$

The amplitude for the production of $T_{cc}^+\pi^+$ from the creation of $D^{*+}D^{*+}$ at short distances is expressed as a loop integral in Eq. (45). Its reduction to the form in Eq. (47) defines the triangle amplitude $T_+(q^2,\gamma^2)$. The first denominator in the loop integral in Eq. (45) can be identified as the denominator of the universal wave function $\psi_T(k_{\rm rel})$ given by Eq. (3), with $\gamma = \sqrt{2\mu(|\varepsilon_T| - i\Gamma_{*+}/2)}$ and the shifted relative momentum $\boldsymbol{k}_{\rm rel} = \boldsymbol{k} + (\mu/M)\boldsymbol{q}$. The universal wave function at the origin is ultraviolet divergent. The regularized wave function $\psi_T^{(\Lambda)}(k_{\rm rel})$ given by Eq. (7) is a simple model with the same momentum dependence as $\psi_T(k_{\rm rel})$ at small $k_{\rm rel}$ but a finite wave function at the origin. The replacement of $\psi_T(k_{\rm rel})$ in the loop integral in Eq. (45) by $\psi_T^{(\Lambda)}(k_{\rm rel})$ can be implemented by making the substitution in Eq. (19). The resulting triangle amplitude for $T_{cc}^+\pi^+$ in the coupled-channel model is

$$T_+^{(\Lambda)}(q^2,\gamma^2) = \frac{\sqrt{(\Lambda+\gamma)\Lambda}}{\sqrt{1+Z_{0+}}(\Lambda-\gamma)}[T_+(q^2,\gamma^2) - T_+(q^2,\Lambda^2)], \tag{B1}$$

where $Z_{0+} = (\Lambda+\gamma)\gamma/[(\Lambda+\gamma_{0+})\gamma_{0+}]$ is the relative probability of the $D^{*0}D^+$ channel. In the expression for $T_+(q^2,\Lambda^2)$, $\sqrt{a+b+c}$ reduces to $i\Lambda$.

2. Amplitude for $T_{cc}^+\pi^-$

Charm mesons $D^{*0}D^{*0}$ created at short distances can rescatter into $T_{cc}^+\pi^-$ through the $D^{*0}D^+$ component of the

T_{cc}^+ wave function. The amplitude for the reaction in XEFT can be represented by the Feynman diagram in Fig. 6 with an appropriate $D^{*0}D^+$-to-T_{cc}^+ vertex. If that vertex is taken to be the same as the $D^{*+}D^0$-to-T_{cc}^+ vertex in Eq. (17), the amplitude for producing $T_{cc}^+\pi^-$ with relative momentum $\boldsymbol{q}$ in their CM frame is

$$\mathcal{A}_{T_{cc}^+\pi^-+y}(\boldsymbol{q}) = i\left(\mathcal{A}^{ij}_{D^{*0}D^{*0}+y}\sqrt{M_T m/M_*^2}\right)4\pi G_\pi M_*\sqrt{\gamma_T}\varepsilon^{i*}\int\frac{d^3k}{(2\pi)^3}\frac{1}{(\boldsymbol{k}+(\mu/M)\boldsymbol{q})^2+\gamma_{0+}^2}\frac{q^j+(m/M_*)k^j}{\boldsymbol{k}^2-(\mu/\mu_\pi)\boldsymbol{q}^2+M_*E_-}, \tag{B2}$$

where $\boldsymbol{\varepsilon}$ is the polarization vector for T_{cc}^+. In the first denominator in the integrand, γ_{0+} is the binding momentum of the $D^{*0}D^+$ channel: $\gamma_{0+}^2 = 2\mu(\delta-\varepsilon_T)$, where $\delta = (M_{*0}+M_+)-(M_{*+}+M_0) = 1.41$ MeV is the energy difference between the $D^{*0}D^+$ and $D^{*+}D^0$ thresholds. Since the real part of that denominator is always greater than $2\mu\delta$, we have omitted its imaginary part. In the second denominator, E_- is the complex energy

$$E_- = \delta + \delta_{+-} - \varepsilon_T - i\Gamma_{*0}, \tag{B3}$$

where $\delta_{+-} = M_{*0} - M_+ - m_- = -2.38$ MeV.

After evaluating the integral over the loop momentum, the amplitude for producing $T_{cc}^+\pi^-$ can be reduced to the form

$$\mathcal{A}_{T_{cc}^+\pi^-+y}(\boldsymbol{q}) = -G_\pi\sqrt{M_T m\gamma_T/4}\,\mathcal{A}^{ij}_{D^{*0}D^{*0}+y}\varepsilon^{i*}q^j T_-(q^2,\gamma_{0+}^2). \tag{B4}$$

The triangle amplitude $T_-(q^2,\gamma_{0+}^2)$ is given by the right side of Eq. (49) with the coefficients

$$a = (\mu/\mu_\pi)q^2 - M_*E_-, \tag{B5a}$$

$$b = -2(\mu/\mu_\pi)(\mu/M)q^2 + M_*E_- - \gamma_{0+}^2, \tag{B5b}$$

$$c = (\mu/M)^2q^2. \tag{B5c}$$

The square root of their sum is $\sqrt{a+b+c} = i\gamma_{0+}$. The triangle amplitude $T_-(q^2,\gamma_{0+}^2)$ can be obtained from $T_+(q^2,\gamma^2)$ by replacing γ^2 by γ_{0+}^2 and replacing E_+ by E_-.

The first denominator in the integrand in Eq. (B2) can be identified as the denominator of the simple wave function $\psi_{0+}(k_{\rm rel})$ for the $D^{*0}D^+$ component of T_{cc}^+ given by Eq. (10), with $\gamma_{\rm cc} = \gamma_{0+}$ and the shifted relative momentum $\boldsymbol{k}_{\rm rel} = \boldsymbol{k} + (\mu/M)\boldsymbol{q}$. The simple wave function at the origin is ultraviolet divergent. The wave function $\psi_{0+}^{(\Lambda)}(k_{\rm rel})$ given by Eq. (11) has the same momentum dependence as $\psi_{0+}(k_{\rm rel})$ at small $k_{\rm rel}$, and it has a finite wave function at the origin that is equal to that for $\psi_T^{(\Lambda)}(k_{\rm rel})$. The replacement of $\psi_{0+}(k_{\rm rel})$ by $\psi_{0+}^{(\Lambda)}(k_{\rm rel})$ can be implemented by making the substitution in Eq. (20) in the amplitude in Eq. (B2). The resulting triangle amplitude in the coupled-channel model is

$$T_-^{(\Lambda)}(q^2,\gamma_{0+}^2) = -\frac{\sqrt{(\Lambda+\gamma)\Lambda}}{\sqrt{1+Z_{0+}}(\Lambda-\gamma_{0+})}\times[T_-(q^2,\gamma_{0+}^2) - T_-(q^2,\Lambda^2)]. \tag{B6}$$

3. Amplitude for $T_{cc}^+\pi^0$

The amplitude in XEFT for the production of $T_{cc}^+\pi^0$ from the creation of $D^{*+}D^{*0}$ at short distances can be expressed as a loop integral analogous to that for $T_{cc}^+\pi^+$ in Eq. (45). The amplitude can be reduced to the expression in Eq. (53), which defines the triangle amplitude $T_0(q^2,\gamma^2)$. The first denominator in Eq. (45) can be identified as the denominator of the universal wave function $\psi_T(k_{\rm rel})$ for the $D^{*+}D^0$ component of the T_{cc}^+. The replacement of $\psi_T(k_{\rm rel})$ in the loop integral by the regularized wave function $\psi_T^{(\Lambda)}(k_{\rm rel})$ can be implemented by making the substitution in Eq. (19). The resulting contribution to the triangle amplitude for $T_{cc}^+\pi^0$ in the coupled-channel model from the $D^{*+}D^0$ component of the T_{cc}^+ wave function is

$$T_0^{(\Lambda)}(q^2,\gamma^2) = \frac{\sqrt{(\Lambda+\gamma)\Lambda}}{\sqrt{1+Z_{0+}}(\Lambda-\gamma)}[T_0(q^2,\gamma^2) - T_0(q^2,\Lambda^2)]. \tag{B7}$$

The production of $T_{cc}^+\pi^0$ can also proceed by the creation of $D^{*0}D^{*+}$ at short distances and their rescattering into $T_{cc}^+\pi^0$ through the $D^{*0}D^+$ component of the T_{cc}^+ wave function. The amplitude for the reaction can be represented by the Feynman diagram in Fig. 6 with an appropriate $D^{*0}D^+$-to-T_{cc}^+ vertex. If that vertex is taken to be the same as the $D^{*+}D^0$-to-T_{cc}^+ vertex in Eq. (17), the contribution $\mathcal{A}'_{T_{cc}^+\pi^0+y}(\boldsymbol{q})$ to the amplitude for producing $T_{cc}^+\pi^0$ with relative momentum $\boldsymbol{q}$ in their CM frame has a form analogous to that in Eq. (B2). It can be reduced to

$$\mathcal{A}'_{T_{cc}^+\pi^0+y}(\boldsymbol{q}) = G_\pi\sqrt{M_T m\gamma_T/8}\,\mathcal{A}^{ij}_{D^{*0}D^{*+}+y}\varepsilon^{i*}q^j T_0(q^2,\gamma_{0+}^2). \tag{B8}$$

The triangle amplitude $T_0(q^2,\gamma_{0+}^2)$ can be obtained from $T_0(q^2,\gamma^2)$ by replacing γ^2 by γ_{0+}^2.

The first denominator in the integrand analogous to that in Eq. (B2) can be identified as the denominator of the simple wave function $\psi_{0+}(k_{\rm rel})$ for the $D^{*0}D^+$ component of T_{cc}^+. The replacement of $\psi_{0+}(k_{\rm rel})$ by $\psi_{0+}^{(\Lambda)}(k_{\rm rel})$ can be implemented by making the substitution in Eq. (20). The triangle amplitude for $T_{cc}^+\pi^0$ in the coupled-channel model from the $D^{*0}D^+$ component of the T_{cc}^+ wave function is

$$T_0'^{(\Lambda)}(q^2,\gamma_{0+}^2) = -\frac{\sqrt{(\Lambda+\gamma)\Lambda}}{\sqrt{1+Z_{0+}}(\Lambda-\gamma_{0+})} \times [T_0(q^2,\gamma_{0+}^2) - T_0(q^2,\Lambda^2)]. \quad \text{(B9)}$$

It can be obtained from $T_0^{(\Lambda)}(q^2,\gamma^2)$ in Eq. (B9) by replacing $T_0(q^2,\gamma^2)$ by $T_0(q^2,\gamma_{0+}^2)$, replacing $1/(\Lambda-\gamma)$ by $1/(\Lambda-\gamma_{0+})$, and multiplying by an overall minus sign.

4. Large q^2

The behavior of the triangle amplitude $T_+^{(\Lambda)}(q^2,\gamma^2)$ defined in Eq. (B1) at large q^2 can be determined by inserting the asymptotic result for $T_+(q^2,\gamma^2)$ in Eq. (A3). The subtraction cancels the terms that decrease as $1/q$, so the triangle amplitude decreases as $1/q^2$,

$$T_+^{(\Lambda)}(q^2,\gamma^2) \to i\frac{2\sqrt{(\Lambda+\gamma)\Lambda}M_T m}{\sqrt{1+Z_{0+}}M_*^2 q^2}. \quad \text{(B10)}$$

This can be expressed in a form with a factor of the regularized wave function at the origin $\psi_T^{(\Lambda)}(r=0)$ given by Eq. (9),

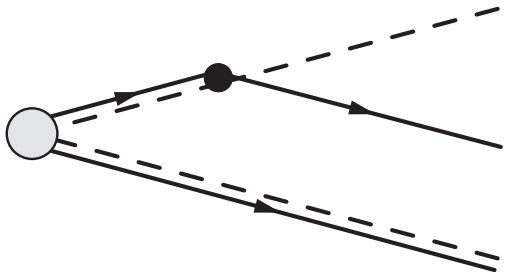

FIG. 13. Feynman diagram in XEFT for $D^{*+}D^{*+}$ created at a point to produce $D^{*+}D^0\pi^+$.

$$T_+^{(\Lambda)}(q^2,\gamma^2) \to i\frac{4\mu_{\pi T}}{M_*\sqrt{\gamma_T/2\pi}}\frac{\psi_T^{(\Lambda)}(r=0)}{\sqrt{1+Z_{0+}}}\frac{1}{q^2}. \quad \text{(B11)}$$

We verify below that this gives the large-q^2 limit for a general wave function with a finite wave function at the origin.

The triangle amplitude $T_+(q^2,\gamma^2)$ for $T_{cc}^+\pi^+$ in Eq. (49) was derived from the loop diagram in Fig. 6. An alternative expression for $T_+(q^2,\gamma^2)$ can be derived from the tree diagram for the production of $D^{*+}D^0\pi^+$ in Fig. 13 along with the wave function $\psi(k)$ for the T_{cc}^+ bound state. We take the momentum of π^+ in the $D^{*+}D^0\pi^+$ CM frame to be $\boldsymbol{q}$. We take the relative momentum of $D^{*+}D^0$ in their CM frame to be $\boldsymbol{k}$. The momentum of D^{*+} and D^0 in the $D^{*+}D^0\pi^+$ CM frame are then $-(M_*/M_T)\boldsymbol{q}+\boldsymbol{k}$ and $-(M/M_T)\boldsymbol{q}-\boldsymbol{k}$. The amplitude for producing $T_{cc}^+\pi^+$ with polarization vector $\boldsymbol{\varepsilon}$ plus additional particles y can be obtained from the amplitude for producing $D^{*+}D^0\pi^+$ by multiplying it by the wave function $\psi(k)$ and integrating over $\boldsymbol{k}$,

$$\mathcal{A}_{T_{cc}^+\pi^+ +y}(\boldsymbol{q}) = i\left(\mathcal{A}^{ij}_{D^{*+}D^{*+}+y}\sqrt{M_T m/M_*^2}\right)\sqrt{8\pi}G_\pi\mu_{\pi T}\varepsilon^{i*}\int\frac{d^3k}{(2\pi)^3}\psi(k)\frac{q^j+(m/2\mu)k^j}{(\boldsymbol{q}+(m/2\mu)\boldsymbol{k})^2-(m/2\mu)M_T(\delta_{0+}-i\Gamma_{*+}/2)}. \quad \text{(B12)}$$

A similar expression involving the universal wave function in Eq. (3) can be obtained from Eq. (45) by making the momentum shift $\boldsymbol{k}\to\boldsymbol{k}-(\mu/M)\boldsymbol{q}$. The terms in the denominator of the integrand proportional to $\boldsymbol{q}^2$, $\boldsymbol{q}\cdot\boldsymbol{k}$, and δ_{0+} agree with those in Eq. (B12). The terms proportional to $\boldsymbol{k}^2$, ε_T, and Γ_{*+} have different coefficients. The amplitude therefore agrees with Eq. (B12) through next-to-leading order in the expansion in power of $1/q$.

We now consider the amplitude in Eq. (B12) at large q^2. We assume $\psi(k)$ decreases rapidly enough for k beyond some momentum scale Λ that its integral over $\boldsymbol{k}$ converges. We take q^2 to be much larger than Λ^2 and also much larger than $m\delta_{0+}$. In that case, we can take the limit $\boldsymbol{k}\to 0$ in the denominator of Eq. (B12) and in the pion emission factor. The amplitude reduces to

$$\mathcal{A}_{T_{cc}^+\pi^+ +y}(\boldsymbol{q}) \to i\left(\mathcal{A}^{ij}_{D^{*+}D^{*+}+y}\sqrt{M_T m/M_*^2}\right) \times \varepsilon^{i*}q^j\frac{\sqrt{8\pi}G_\pi\mu_{\pi T}}{q^2}\psi(r=0). \quad \text{(B13)}$$

By comparing this to Eq. (47), we can verify that the large-q^2 limit of $T_+(q^2,\gamma^2)$ is given up to a sign by Eq. (B11) with $\psi_T^{(\Lambda)}(r=0)/\sqrt{1+Z_{0+}}$ replaced by $\psi(r=0)$.

[1] F. K. Guo, C. Hanhart, U. G. Meißner, Q. Wang, Q. Zhao, and B. S. Zou, Hadronic molecules, Rev. Mod. Phys. **90**, 015004 (2018).

[2] A. Ali, J. S. Lange, and S. Stone, Exotics: Heavy pentaquarks and tetraquarks, Prog. Part. Nucl. Phys. **97**, 123 (2017).

[3] S. L. Olsen, T. Skwarnicki, and D. Zieminska, Nonstandard heavy mesons and baryons: Experimental evidence, Rev. Mod. Phys. **90**, 015003 (2018).

[4] M. Karliner, J. L. Rosner, and T. Skwarnicki, Multiquark states, Annu. Rev. Nucl. Part. Sci. **68**, 17 (2018).

[5] C. Z. Yuan, The XYZ states revisited, Int. J. Mod. Phys. A **33**, 1830018 (2018).

[6] Y. R. Liu, H. X. Chen, W. Chen, X. Liu, and S. L. Zhu, Pentaquark and tetraquark states, Prog. Part. Nucl. Phys. **107**, 237 (2019).

[7] N. Brambilla, S. Eidelman, C. Hanhart, A. Nefediev, C. P. Shen, C. E. Thomas, A. Vairo, and C. Z. Yuan, The XYZ states: Experimental and theoretical status and perspectives, Phys. Rep. **873**, 1 (2020).

[8] S. K. Choi *et al.* (Belle Collaboration), Observation of a Narrow Charmonium-Like State in Exclusive $B^{\pm} \to K^{\pm}\pi^{+}\pi^{-}J/\psi$ Decays, Phys. Rev. Lett. **91**, 262001 (2003).

[9] R. Aaij *et al.* (LHCb Collaboration), Observation of an exotic narrow doubly charmed tetraquark, Nat. Phys. **18**, 751 (2022).

[10] R. Aaij *et al.* (LHCb Collaboration), Study of the doubly charmed tetraquark T_{cc}^{+}, Nat. Commun. **13**, 3351 (2022).

[11] J. J. Aubert *et al.* (E598 Collaboration), Experimental Observation of a Heavy Particle J, Phys. Rev. Lett. **33**, 1404 (1974).

[12] J. E. Augustin *et al.* (SLAC-SP-017 Collaboration), Discovery of a Narrow Resonance in $e^{+}e^{-}$ Annihilation, Phys. Rev. Lett. **33**, 1406 (1974).

[13] M. Gell-Mann, A schematic model of baryons, and mesons, Phys. Lett. **8**, 214 (1964).

[14] G. Zweig, An SU(3) model for strong interaction symmetry and its breaking. Version 1, Report No. CERN-TH-401, 1964, http://cds.cern.ch/record/352337; An SU(3) model for strong interaction symmetry and its breaking. Version 2, Report No. CERN-TH-412, 1964, http://cds.cern.ch/record/570209.

[15] R. Aaij *et al.* (LHCb Collaboration), Study of the lineshape of the $\chi_{c1}(3872)$ state, Phys. Rev. D **102**, 092005 (2020).

[16] R. Aaij *et al.* (LHCb Collaboration), Study of the $\psi_2(3823)$ and $\chi_{c1}(3872)$ states in $B^{+} \to (J\psi\pi^{+}\pi^{-})K^{+}$ decays, J. High Energy Phys. 08 (2020) 123.

[17] R. Aaij *et al.* (LHCb Collaboration), Determination of the $X(3872)$ Meson Quantum Numbers, Phys. Rev. Lett. **110**, 222001 (2013).

[18] E. Braaten and H.-W. Hammer, Universality in few-body systems with large scattering length, Phys. Rep. **428**, 259 (2006).

[19] E. Braaten and M. Kusunoki, Low-energy universality and the new charmonium resonance at 3870 MeV, Phys. Rev. D **69**, 074005 (2004).

[20] L. Meng, G. J. Wang, B. Wang, and S. L. Zhu, Probing the long-range structure of the T_{cc}^{+} with the strong and electromagnetic decays, Phys. Rev. D **104**, L051502 (2021).

[21] X. Z. Ling, M. Z. Liu, L. S. Geng, E. Wang, and J. J. Xie, Can we understand the decay width of the T_{cc}^{+} state?, Phys. Lett. B **826**, 136897 (2022).

[22] M. J. Yan and M. P. Valderrama, Subleading contributions to the decay width of the T_{cc}^{+} tetraquark, Phys. Rev. D **105**, 014007 (2022).

[23] S. Fleming, R. Hodges, and T. Mehen, T_{cc}^{+} decays: Differential spectra and two-body final states, Phys. Rev. D **104**, 116010 (2021).

[24] H. Ren, F. Wu, and R. Zhu, Hadronic molecule interpretation of T_{cc}^{+} and its beauty-partners, Adv. High Energy Phys. **2022**, 910303 (2022).

[25] A. Feijoo, W. H. Liang, and E. Oset, $D^{0}D^{0}\pi^{+}$ mass distribution in the production of the T_{cc} exotic state, Phys. Rev. D **104**, 114015 (2021).

[26] L. Y. Dai, X. Sun, X. W. Kang, A. P. Szczepaniak, and J. S. Yu, Pole analysis on the doubly charmed meson in $D^{0}D^{0}\pi^{+}$ mass spectrum, Phys. Rev. D **105**, L051507 (2022).

[27] M. Albaladejo, T_{cc}^{+} coupled channel analysis and predictions, Phys. Lett. B **829**, 137052 (2022).

[28] M. L. Du, V. Baru, X. K. Dong, A. Filin, F. K. Guo, C. Hanhart, A. Nefediev, J. Nieves, and Q. Wang, Coupled-channel approach to T_{cc}^{+} including three-body effects, Phys. Rev. D **105**, 014024 (2022).

[29] Q. Qin, Y. F. Shen, and F. S. Yu, Discovery potentials of double-charm tetraquarks, Chin. Phys. C **45**, 103106 (2021).

[30] Y. Jin, S. Y. Li, Y. R. Liu, Q. Qin, Z. G. Si, and F. S. Yu, Colour and baryon number fluctuation of preconfinement system in production process and T_{cc} structure, Phys. Rev. D **104**, 114009 (2021).

[31] S. Cho and S. H. Lee, Hadronic effects on the X(3872) meson abundance in heavy ion collisions, Phys. Rev. C **88**, 054901 (2013).

[32] A. Martinez Torres, K. P. Khemchandani, F. S. Navarra, M. Nielsen, and L. M. Abreu, On $X(3872)$ production in high energy heavy ion collisions, Phys. Rev. D **90**, 114023 (2014); **93**, 059902(E) (2016).

[33] L. M. Abreu, K. P. Khemchandani, A. Martinez Torres, F. S. Navarra, and M. Nielsen, $X(3872)$ production and absorption in a hot hadron gas, Phys. Lett. B **761**, 303 (2016).

[34] H. Zhang, J. Liao, E. Wang, Q. Wang, and H. Xing, Deciphering the Nature of X(3872) in Heavy Ion Collisions, Phys. Rev. Lett. **126**, 012301 (2021).

[35] B. Wu, X. Du, M. Sibila, and R. Rapp, $X(3872)$ transport in heavy-ion collisions, Eur. Phys. J. A **57**, 122 (2021); **57**, 314 (E) (2021).

[36] B. Chen, L. Jiang, X. H. Liu, Y. Liu, and J. Zhao, X(3872) production in relativistic heavy-ion collisions, Phys. Rev. C **105**, 054901 (2022).

[37] J. Hong, S. Cho, T. Song, and S. H. Lee, Hadronic effects on the $cc\bar{q}\,\bar{q}$ tetraquark state in relativistic heavy ion collisions, Phys. Rev. C **98**, 014913 (2018).

[38] C. E. Fontoura, G. Krein, A. Valcarce, and J. Vijande, Production of exotic tetraquarks $QQ\bar{q}\,\bar{q}$ in heavy-ion collisions at the LHC, Phys. Rev. D **99**, 094037 (2019).

[39] Y. Hu, J. Liao, E. Wang, Q. Wang, H. Xing, and H. Zhang, The production of doubly charmed exotic hadrons in heavy ion collisions, Phys. Rev. D **104**, L111502 (2021).

[40] L. M. Abreu, F. S. Navarra, M. Nielsen, and H. P. L. Vieira, Interactions of the doubly charmed state T_{cc}^{+} with a hadronic medium, Eur. Phys. J. C **82**, 296 (2022).
[41] R. Karplus, C. M. Sommerfield, and E. H. Wichmann, Spectral representations in perturbation theory. 1. Vertex function, Phys. Rev. **111**, 1187 (1958).
[42] L. D. Landau, On analytic properties of vertex parts in quantum field theory, Nucl. Phys. **13**, 181 (1959).
[43] A. P. Szczepaniak, Triangle singularities and XYZ quarkonium peaks, Phys. Lett. B **747**, 410 (2015).
[44] X. H. Liu, M. Oka, and Q. Zhao, Searching for observable effects induced by anomalous triangle singularities, Phys. Lett. B **753**, 297 (2016).
[45] E. Braaten, L.-P. He, and K. Ingles, Production of $X(3872)$ accompanied by a pion in B meson decay, Phys. Rev. D **100**, 074028 (2019).
[46] E. Braaten, L.-P. He, and K. Ingles, Production of $X(3872)$ accompanied by a soft pion at hadron colliders, Phys. Rev. D **100**, 094006 (2019).
[47] F. K. Guo, Novel Method for Precisely Measuring the $X(3872)$ Mass, Phys. Rev. Lett. **122**, 202002 (2019).
[48] S. Sakai, E. Oset, and F. K. Guo, Triangle singularity in the $B^{-} \to K^{-}\pi^{0}X(3872)$ reaction and sensitivity to the $X(3872)$ mass, Phys. Rev. D **101**, 054030 (2020).
[49] S. Sakai, H. J. Jing, and F. K. Guo, Possible precise measurements of the $X(3872)$ mass with the $e^{+}e^{-} \to \pi^{0}\gamma X(3872)$ and $p\bar{p} \to \gamma X(3872)$ reactions, Phys. Rev. D **102**, 114041 (2020).
[50] S. Dubynskiy and M. B. Voloshin, $e^{+}e^{-} \to \gamma X(3872)$ near the $D^{*}\bar{D}^{*}$ threshold, Phys. Rev. D **74**, 094017 (2006).
[51] E. Braaten, L.-P. He, and K. Ingles, Triangle singularity in the production of $X(3872)$ and a photon in $e^{+}e^{-}$ annihilation, Phys. Rev. D **100**, 031501 (2019).
[52] E. Braaten, L.-P. He, and K. Ingles, Production of $X(3872)$ and a photon in $e^{+}e^{-}$ annihilation, Phys. Rev. D **101**, 014021 (2020).
[53] R. Molina and E. Oset, Triangle singularity in $B^{-} \to K^{-}X(3872)$; $X \to \pi^{0}\pi^{+}\pi^{-}$ and the X(3872) mass, Eur. Phys. J. C **80**, 451 (2020).
[54] S. X. Nakamura, Triangle singularity appearing as an $X(3872)$-like peak in $B \to (J/\psi\pi^{+}\pi^{-})K\pi$, Phys. Rev. D **102**, 074004 (2020).
[55] E. Braaten, L.-P. He, K. Ingles, and J. Jiang, Charm-meson triangle singularity in $e^{+}e^{-}$ annihilation into $D^{*0}\bar{D}^{0} + \gamma$, Phys. Rev. D **101**, 096020 (2020).
[56] M. Suzuki, The X(3872) boson: Molecule or charmonium, Phys. Rev. D **72**, 114013 (2005).
[57] S. Fleming, M. Kusunoki, T. Mehen, and U. van Kolck, Pion interactions in the $X(3872)$, Phys. Rev. D **76**, 034006 (2007).
[58] E. Braaten, Galilean-invariant effective field theory for the $X(3872)$, Phys. Rev. D **91**, 114007 (2015).
[59] E. Braaten, L.-P. He, and J. Jiang, Galilean-invariant effective field theory for the $X(3872)$ at next-to-leading order, Phys. Rev. D **103**, 036014 (2021).
[60] E. Braaten, H.-W. Hammer, and T. Mehen, Scattering of an ultrasoft pion and the $X(3872)$, Phys. Rev. D **82**, 034018 (2010).
[61] M. Butenschoen, Z. G. He, and B. A. Kniehl, NLO NRQCD disfavors the interpretation of X(3872) as $\chi_{c1}(2P)$, Phys. Rev. D **88**, 011501 (2013).
[62] C. Meng, H. Han, and K. T. Chao, X(3872) and its production at hadron colliders, Phys. Rev. D **96**, 074014 (2017).
[63] M. Butenschoen, Z. G. He, and B. A. Kniehl, Deciphering the $X(3872)$ via Its Polarization in Prompt Production at the CERN LHC, Phys. Rev. Lett. **123**, 032001 (2019).
[64] C. Bignamini, B. Grinstein, F. Piccinini, A. D. Polosa, and C. Sabelli, Is the X(3872) Production Cross Section at Tevatron Compatible with a Hadron Molecule Interpretation?, Phys. Rev. Lett. **103**, 162001 (2009).
[65] P. Artoisenet and E. Braaten, Production of the X(3872) at the Tevatron and the LHC, Phys. Rev. D **81**, 114018 (2010).
[66] M. Albaladejo, F. K. Guo, C. Hanhart, U. G. Meißner, J. Nieves, A. Nogga, and Z. Yang, Note on X(3872) production at hadron colliders and its molecular structure, Chin. Phys. C **41**, 121001 (2017).
[67] E. Braaten, L. P. He, and K. Ingles, Estimates of the $X(3872)$ cross section at a hadron collider, Phys. Rev. D **100**, 094024 (2019).
[68] A. Esposito, E. G. Ferreiro, A. Pilloni, A. D. Polosa, and C. A. Salgado, The nature of $X(3872)$ from high-multiplicity pp collisions, Eur. Phys. J. C **81**, 669 (2021).
[69] R. Aaij *et al.* (LHCb Collaboration), Observation of Multiplicity Dependent Prompt $\chi_{c1}(3872)$ and $\psi(2S)$ Production in pp Collisions, Phys. Rev. Lett. **126**, 092001 (2021).
[70] E. Braaten, L.-P. He, K. Ingles, and J. Jiang, Production of $X(3872)$ at high multiplicity, Phys. Rev. D **103**, L071901 (2021).
[71] E. Braaten and M. Kusunoki, Factorization in the production and decay of the $X(3872)$, Phys. Rev. D **72**, 014012 (2005).
[72] C. Schmid, Final-state interactions and the simulation of resonances, Phys. Rev. **154**, 1363 (1967).